Universiteit
Leiden
The Netherlands

Novel mediators of anti-tumor immunity: dissecting intratumoral immune responses at the single-cell level

Vries, N.L. de

Citation

Vries, N. L. de. (2022, October 6). *Novel mediators of anti-tumor immunity: dissecting intratumoral immune responses at the single-cell level*. Retrieved from https://hdl.handle.net/1887/3439882

Version:	Publisher's Version
License:	Licence agreement concerning inclusion of doctoral thesis in the Institutional Repository of the University of Leiden
Downloaded from:	https://hdl.handle.net/1887/3439882

Note: To cite this publication please use the final published version (if applicable).

High-dimensional cytometric analysis of colorectal cancer reveals novel mediators of anti-tumor immunity

3

Natasja L. de Vries[1,2], Vincent van Unen[2#], Marieke E. Ijsselsteijn[1#], Tamim Abdelaal[3,4#], Ruud van der Breggen[1], Arantza Farina Sarasqueta[1], Ahmed Mahfouz[3,4], Koen C.M.J. Peeters[5], Thomas Höllt[4,6], Boudewijn P.F. Lelieveldt[3,7], Frits Koning[2†], Noel F.C.C. de Miranda[1†].

[1]Department of Pathology, Leiden University Medical Center, Leiden, the Netherlands. [2]Department of Immunology, Leiden University Medical Center, Leiden, the Netherlands. [3]Department of Pattern Recognition and Bioinformatics, Delft University of Technology, Delft, the Netherlands. [4]Leiden Computational Biology Center, Leiden University Medical Center, Leiden, the Netherlands. [5]Department of Surgery, Leiden University Medical Center, Leiden, the Netherlands. [6]Computer Graphics and Visualization, Delft University of Technology, Delft, the Netherlands. [7]Department of LKEB Radiology, Leiden University Medical Center, Leiden, the Netherlands. [#]Equal contribution to this study. [†]Equal responsible authors.

Gut. 2020; 69: 691-703.
doi: 10.1136/gutjnl-2019-318672

ABSTRACT

Objective

A comprehensive understanding of anti-cancer immune responses is paramount for the optimal application and development of cancer immunotherapies. We unraveled local and systemic immune profiles in colorectal cancer (CRC) patients by high-dimensional analysis to provide an unbiased characterization of the immune contexture of CRC.

Design

Thirty-six immune cell markers were simultaneously assessed at the single-cell level by mass cytometry in 35 CRC tissues, 26 tumor-associated lymph nodes, 17 colorectal healthy mucosa, and 19 peripheral blood samples from 31 CRC patients. Additionally, functional, transcriptional, and spatial analyses of tumor-infiltrating lymphocytes were performed by flow cytometry, single-cell RNA-sequencing, and multispectral immunofluorescence.

Results

We discovered that a previously unappreciated innate lymphocyte population ($Lin^-CD7^+CD127^-CD56^+CD45RO^+$) was enriched in CRC tissues and displayed cytotoxic activity. This subset demonstrated a tissue-resident ($CD103^+CD69^+$) phenotype, and was most abundant in immunogenic mismatch repair (MMR)-deficient CRCs. Their presence in tumors was correlated with the infiltration of tumor-resident cytotoxic, helper, and γδ T cells with highly similar activated ($HLA\text{-}DR^+CD38^+PD\text{-}1^+$) phenotypes. Remarkably, activated γδ T cells were almost exclusively found in MMR-deficient cancers. Non-activated counterparts of tumor-resident cytotoxic and γδ T cells were present in CRC and healthy mucosa tissues, but not in lymph nodes, with the exception of tumor-positive lymph nodes.

Conclusion

This work provides a blueprint for the understanding of the heterogeneous and intricate immune landscape of CRC, including the identification of previously unappreciated immune cell subsets. The concomitant presence of tumor-resident innate and adaptive immune cell populations suggests a multi-targeted exploitation of their anti-tumor properties in a therapeutic setting.

INTRODUCTION

T cell checkpoint blockade immunotherapies have revolutionized cancer treatment following the clinical success achieved with therapeutic antibodies targeting CTLA-4 and the PD-1/PD-L1 axis in cancer patients. These strategies reinvigorate anti-tumor T cell responses, and are particularly effective in cancers with high mutation burden like melanomas, non-small cell lung cancers, and DNA mismatch repair (MMR)-deficient cancers.[1-5] MMR deficiency occurs in approximately 15-20% of colorectal cancers (CRCs) and leads to the widespread accumulation of somatic mutations in tumors, including insertions and deletions at DNA microsatellite sequences.[6,7] Such a theoretically immunogenic profile is corroborated by the presence of numerous intraepithelial lymphocytes in these cancers, in contrast to MMR-proficient cancers.[8,9] Nevertheless, not all MMR-deficient CRCs respond to immune checkpoint blockade, while MMR-proficient CRCs are insensitive to this therapy.

To understand the mechanisms that determine responses to current immunotherapies and for the design of alternative approaches, it is crucial to characterize the cancer microenvironment with multidimensional approaches that allow the simultaneous identification and characterization of immune cell populations across multiple lineages.[10,11] Mass cytometry allows a detailed single-cell characterization of adaptive and innate immune landscapes, thereby providing a unique platform to discriminate immune cell subsets that can be exploited in an immunotherapeutic setting.

We performed an in-depth characterization of immune landscapes across CRC tissues, tumor-associated lymph nodes, colorectal healthy mucosa, and peripheral blood samples from 31 CRC patients by high-dimensional single-cell mass cytometry. We revealed tumor tissue-specific immune signatures across the adaptive and innate compartments, and discovered a previously unappreciated innate immune cell population implicated in anti-tumor immunity that strongly differentiated immunogenic (MMR-deficient) from non-immunogenic (MMR-proficient) CRCs.

RESULTS

Tumor-resident immune cell populations derive from multiple lineages

Mass cytometric analysis of 36 immune cell markers was performed on single-cell suspensions isolated from cancer and healthy tissues of CRC patients (**Table S1, Table S2**). To decipher their immune composition, we performed HSNE analysis in Cytosplore on all acquired $CD45^+$ cells of the discovery cohort ($8.9*10^6$ cells in total) (**Figure 1A, Figure S1**). Based on the density features of the HSNE-embedded landmarks, 7 major immune cell clusters were identified by unsupervised GMS clustering, which corresponded to naive and memory (based on CD45RO and CCR7 expression) $CD4^+$ and $CD8^+/\gamma\delta$ T cells, B cells, Lin^-CD7^+ ILCs, and myeloid cells (**Figure 1A,B**). Memory $CD4^+$ and $CD8^+$ T cells, as well as myeloid cells, were dominant immune lineages in the tumor microenvironment, while B cells, Lin^-CD7^+

ILCs, and naive CD4+ and CD8+ T cells were present at a lower extent (**Figure S2**). The HSNE analysis also unveiled the presence of several tumor tissue-specific, phenotypically distinct landmarks within the memory CD4+ T cell, CD8+/γδ T cell, Lin−CD7+ ILC, and myeloid cell compartments (**Figure 1A**).

All 7 major immune lineages were analyzed in detail by hierarchical exploration of the data in HSNE. As an example, the embedding of the memory CD8+/γδ T cell compartment is shown in **Figure 1C**. Altogether, analysis of these 7 major immune lineages yielded 220 distinct immune cell clusters, of which 2 consisted of less than 100 cells and were excluded from further analysis. All acquired CD45+ cells of the validation cohort ($6.6*10^6$ cells in total) were subsequently classified into these pre-identified immune cell clusters based on their phenotype (see **Methods**).

The mass cytometric analysis was accompanied by single-cell RNA-sequencing of CD45+ cells from 7 CRC tissues. Seven immune cell clusters could be detected based on transcriptomic profiles (**Figure 1D**), corresponding to B cells, CD8+ and CD4+ T cells, ILCs, myeloid cells, proliferating cells, and plasma B cells (**Figure 1D,E**).

Activated CD8+ and γδ T cells are tumor tissue-specific and enriched in mismatch repair-deficient colorectal cancers

Hierarchical clustering analysis revealed that memory CD8+/γδ T cell phenotypes clustered in a tissue-specific manner (**Figure 2A**). Two CD8+CD103+PD-1+ populations (#60 and 96), distinguished by CD161 expression, were present in tumor tissues (constituting up to 28.2% of CD45+ cells) and infrequent in all other samples (**Figure 2B,C**), with the exception of one lymph node sample that was found to be infiltrated by tumor cells upon histological examination (data not shown). These CD8+CD103+PD-1+ cells were further characterized by the co-expression of CD69, FAS, HLA-DR, and CD38 (**Figure 2B**). Interestingly, the CD161− counterpart of CD8+CD103+PD-1+ T cells (#60) was particularly abundant in MMR-deficient tumors as compared to MMR-proficient tumors (**Figure S3**). Within the CD8+CD103+PD-1+CD38+ subset, we observed co-expression of CD39 (**Figure S3**), a marker that has recently been found to identify tumor-reactive CD8+ T cells.[12,13] Next to these tumor-resident cells, a cluster (#61) with a similar phenotype but lacking HLA-DR, PD-1, FAS, and possessing a lower expression of CD38 was present in both tumor and healthy colorectal samples (**Figure 2B,C**), and may represent a non-activated counterpart. Single-cell RNA-sequencing revealed that CD8+ T cells in colorectal tumors expressed cytolytic molecules (e.g. *GZMA*, *GZMB*, *GZMH, PRF1*) (**Figure 2D**). Furthermore, they displayed expression of the immune checkpoint molecule *LAG3* (**Figure 2D**).

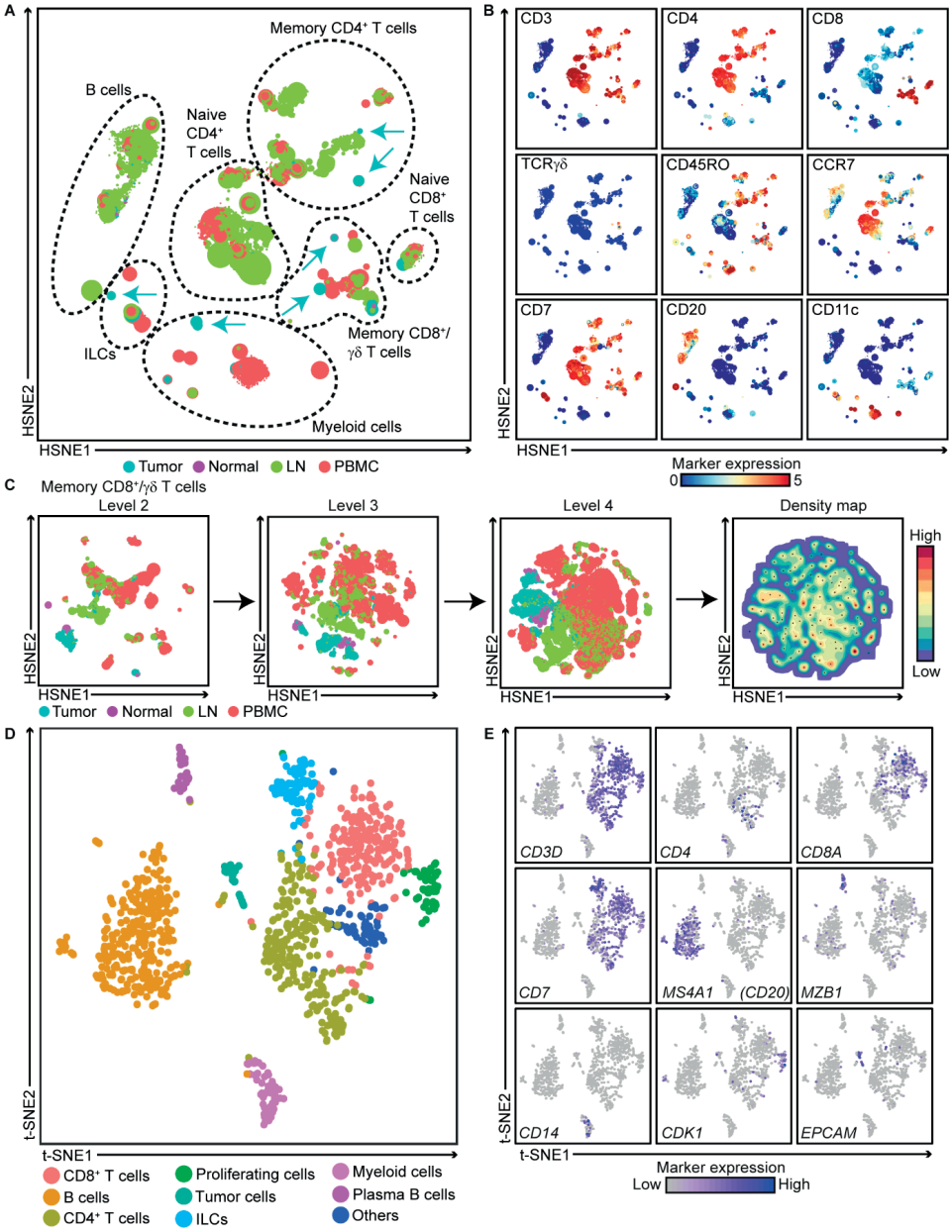

Figure 1. Tumor-resident immune cell populations derive from multiple lineages.
A and B. HSNE embedding showing $7.5*10^4$ landmarks representing immune cells ($8.9*10^6$ cells) isolated from CRC tissues (N=19), tumor-associated lymph nodes (N=17), colorectal healthy mucosa (N=4), and peripheral blood (N=9) samples from the discovery cohort. Colors represent the different tissue types (**A**) and the relative expression of indicated immune lineage markers (**B**). Arrows indicate the HSNE location of phenotypically distinct tumor-resident immune cell populations. **C.** Example of an HSNE analysis of $7.4*10^2$ landmarks representing $1.1*10^6$ cells from the memory CD8⁺/γδ T cell compartment as identified in (**A**). All landmarks are selected and embedded at the next, more detailed levels showing a finer granularity of structures with $5.0x10^3$ landmarks at level 2, to $3.0*10^4$ landmarks at level 3, and $1.6*10^5$ landmarks at level 4. Phenotypically distinct immune cell clusters were identified by unsupervised GMS clustering based on the density features. Black dots indicate the centroids of the identified clusters. **D and E.** t-SNE

embedding showing 1,079 cells from CRC tissues (N=7) analyzed by single-cell RNA-sequencing. Colors represent the different clusters (**D**) and the log-transformed expression levels of indicated immune lineage markers (**E**). Each dot represents a single cell.

Strikingly, a TCRγδ$^+$CD103$^+$PD-1$^+$ population (#99) was almost exclusively found in MMR-deficient tumors, constituting up to 8.4% of CD45$^+$ cells (**Figure 2B,C**). These γδ T cells had a phenotype similar to the CD8$^+$CD103$^+$PD-1$^+$ cells, as defined by co-expression of CD69, FAS, CD38, and HLA-DR (**Figure 2B**). An HLA-DR$^-$PD-1$^-$ counterpart of these cells (#97 and 101) was also observed in colorectal healthy mucosa and MMR-proficient tumors, and may represent a non-activated form of the CD103$^+$PD-1$^+$ γδ T cells in the tumor microenvironment (**Figure 2B,C**). We analyzed the cytotoxic potential of the tumor-resident γδ T cells by flow cytometry and determined that these were capable of producing IFN-γ and granzyme B/perforin upon stimulation with PMA/ionomycin (**Figure S4**).

3

ICOS$^+$ and activated CD4$^+$ T cells are dominant, tumor tissue-specific T cell populations in both mismatch repair-deficient and -proficient colorectal cancers

Next, we determined the cell surface phenotype of memory CD4$^+$ T cells in CRC patients. Memory CD4$^+$ T cells also distributed in a tissue-specific manner (**Figure 3A**). Here, a large population of CD4$^+$ICOS$^+$CD27$^-$ cells (#20 and 58) constituted up to 21.1% of CD45$^+$ cells in CRCs, while being absent in all other tissues with the exception of tumor-positive lymph node samples (**Figure 3B,C**). Part of this population co-expressed CD161 and PD-1 (#58), whereas the other part was negative for these markers but expressed high levels of CD25 (#20), indicative of a regulatory-like phenotype (**Figure 3B**). Flow cytometry analysis confirmed the expression of FOXP3 in 91-98% of ICOS$^+$ CD4$^+$CD45RO$^+$CD25$^+$CD127^{low} T cells in colorectal tumors (**Figure S5**). Interestingly, the ICOS$^+$ CD4$^+$ T cells were present in MMR-deficient as well as MMR-proficient tumors to a similar extent (**Figure 3B,C**).

In addition, CD4$^+$CD103$^+$PD-1$^+$ cells (#85 and 86), which constituted up to 23.8% of CD45$^+$ cells, were also enriched in tumor tissues (**Figure 3B,C**). Strikingly, several features of these cells mirrored our observations in the CD8$^+$/γδ compartment, including a tissue-resident phenotype defined by co-expression of CD69, FAS, CD38, and HLA-DR (**Figure 3B**). Moreover, expression of CD161 also subdivided CD4$^+$CD103$^+$PD-1$^+$ T cells into a positive (#85) and negative (#86) population, where CD161$^-$ cells were more abundant in MMR-deficient as compared to MMR-proficient tumors (**Figure S3**). In contrast to the tumor-resident CD8$^+$ and γδ T cells, a non-activated counterpart could not be detected for these cells.

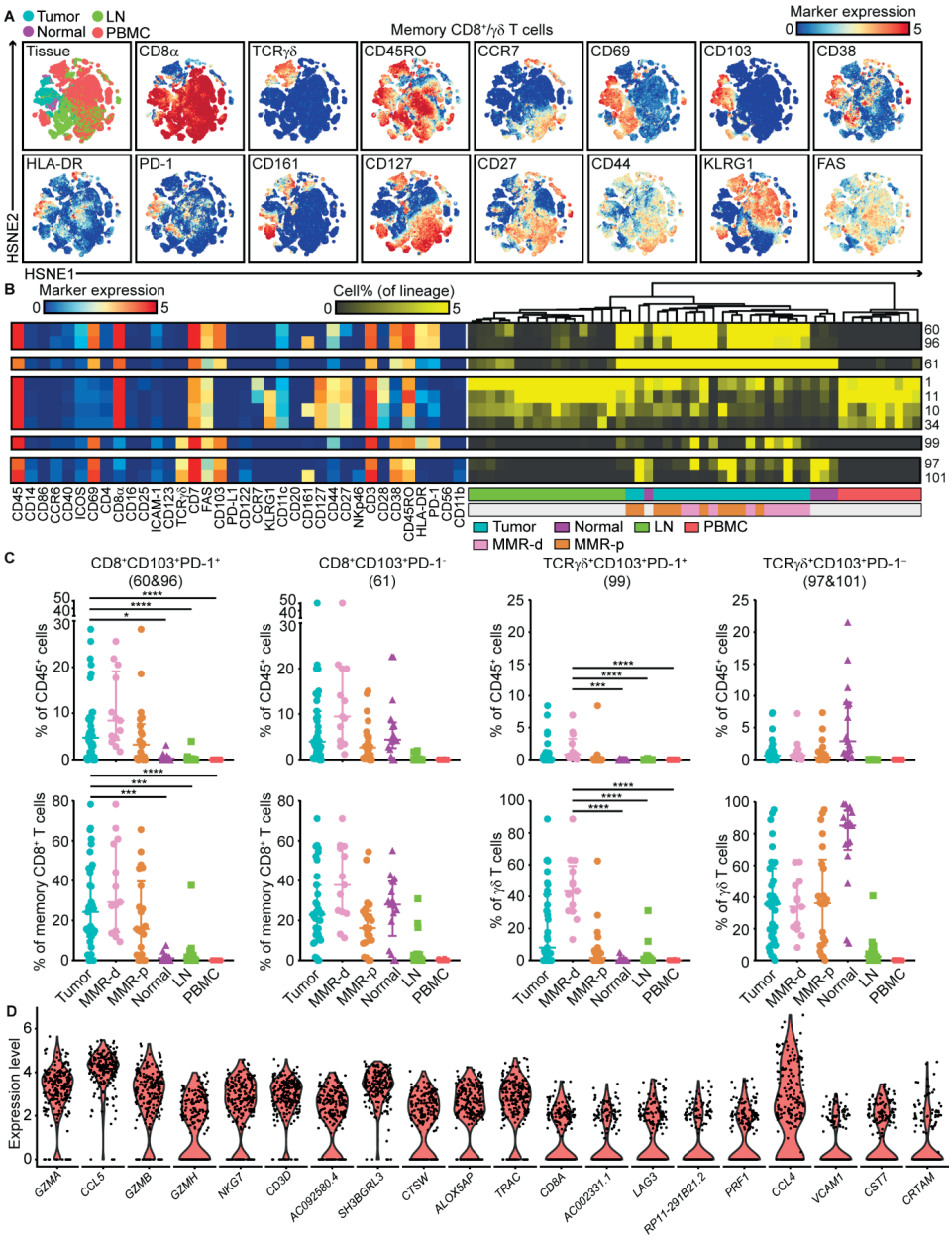

Figure 2. Activated CD8⁺ and γδ T cells are tumor tissue-specific and enriched in mismatch repair-deficient colorectal cancers.

A. HSNE embedding of $1.6*10^5$ landmarks representing the memory CD8⁺/γδ T cell compartment ($1.1*10^6$ cells) from the discovery cohort of CRC patients colored by tissue type (first plot) and relative expression of indicated markers. **B.** A heatmap showing median marker expression values (left) and a heatmap showing frequencies of selected memory CD8⁺/γδ T cell clusters (right). Hierarchical clustering was performed on cluster frequencies using Spearman's rank correlation. Color bars indicate tissue type. **C.** Frequencies of selected memory CD8⁺/γδ T cell clusters among CRC patients' tissues (N=35, further subdivided into MMR-deficient (N=13) and MMR-proficient (N=22)), colorectal healthy mucosa (N=17), tumor-associated lymph nodes (N=26), and peripheral blood (N=19) as percentage of total CD45⁺ cells

(upper panel) and memory CD8$^+$ or γδ T cells (lower panel). Cluster IDs correspond to the ones in (**B**). Bars indicate median ± IQR. Each dot represents an individual sample. Data from 22 independent experiments with mass cytometry. *P<0.05, ***P<0.001, ****P<0.0001 by Kruskal-Wallis test with Dunn's test for multiple comparisons. **D.** Violin plot showing log-transformed expression levels of the top 20 differentially expressed genes within CD8$^+$ T cells (N=217) analyzed by single-cell RNA-sequencing on CD45$^+$ cells from 7 tumors (**Figure 1D**). Each dot represents a single cell.

While ICOS$^+$ regulatory T cells (Tregs) were tumor tissue-specific, ICOS$^-$CD25$^+$CD127$^-$ Tregs (#13-73) were found in both tumor-associated lymph nodes and CRC tissues (**Figure 3B,C**). Lastly, immune cell populations such as CD4$^+$CD27$^+$CD127$^+$ central memory (CCR7$^+$CD45RO$^+$) cells (#1-37) were more abundant in peripheral blood and lymph nodes (**Figure 3B,C**). The expression of *ICOS* on CD4$^+$ T cells was confirmed by single-cell RNA-sequencing, which also revealed the expression of *TNFRSF4 (OX40R)* and *TNFRSF18 (GITR)* (**Figure 3D**). t-SNE analysis revealed the co-expression of all three immunotherapeutic targets by CD4$^+$ T cells (**Figure S6**).

CD127$^-$CD56$^+$CD45RO$^+$ ILCs are the prevalent ILC population in mismatch repair-deficient colorectal tumors

Mass cytometric profiles of the innate lymphoid compartment revealed the presence of three distinct Lin$^-$CD7$^+$ cell clusters: CD127$^-$CD56$^+$CD45RO$^-$ natural killer (NK) cells (90.4%), CD127$^+$ ILCs (3.4%), and a cluster of CD127$^-$CD56$^+$CD45RO$^+$ cells (6.2%) (**Figure 4A**). Analysis of cluster frequencies demonstrated that CD56^{dim}CD16^{bright} NK cells (#33-4) were present in high frequencies in peripheral blood, whereas CD56^{bright}CD16^{dim} NK cells (#10-82) were the dominant NK-type in lymph node samples (**Figure 4B,C**). CD127$^+$ ILCs (#6-9) were more abundant in healthy mucosa, lymph nodes and MMR-proficient tumors, and displayed a KLRG1$^-$ phenotype, characteristic of ILC3 cells (**Figure 4B,C**). Strikingly, the CD127$^-$CD56$^+$CD45RO$^+$ ILCs (#87,95,92,97) were enriched in tumor tissues, accounting for up to 80% of the innate lymphoid compartment (**Figure 4B,C**). Moreover, they were particularly abundant in MMR-deficient tumors, especially CD161$^-$ populations (#95, 92 and 97) (**Figure 4B,C**). The CD127$^-$CD56$^+$CD45RO$^+$ ILC population has recently been identified in human fetal intestine as intermediate-ILCs.[14] Consistent with that work, hierarchical clustering positioned the CD127$^-$CD56$^+$CD45RO$^+$ ILCs in between NK cells and CD127$^+$ ILCs (**Figure 4B**). We observed co-expression of CD69 and CD103 on all CD127$^-$CD56$^+$CD45RO$^+$ ILCs, but differential expression of CD16, ICAM-1, FAS, CD11c, CD161, CD44 and HLA-DR, indicative of further heterogeneity within this cell cluster (**Figure 4B**).

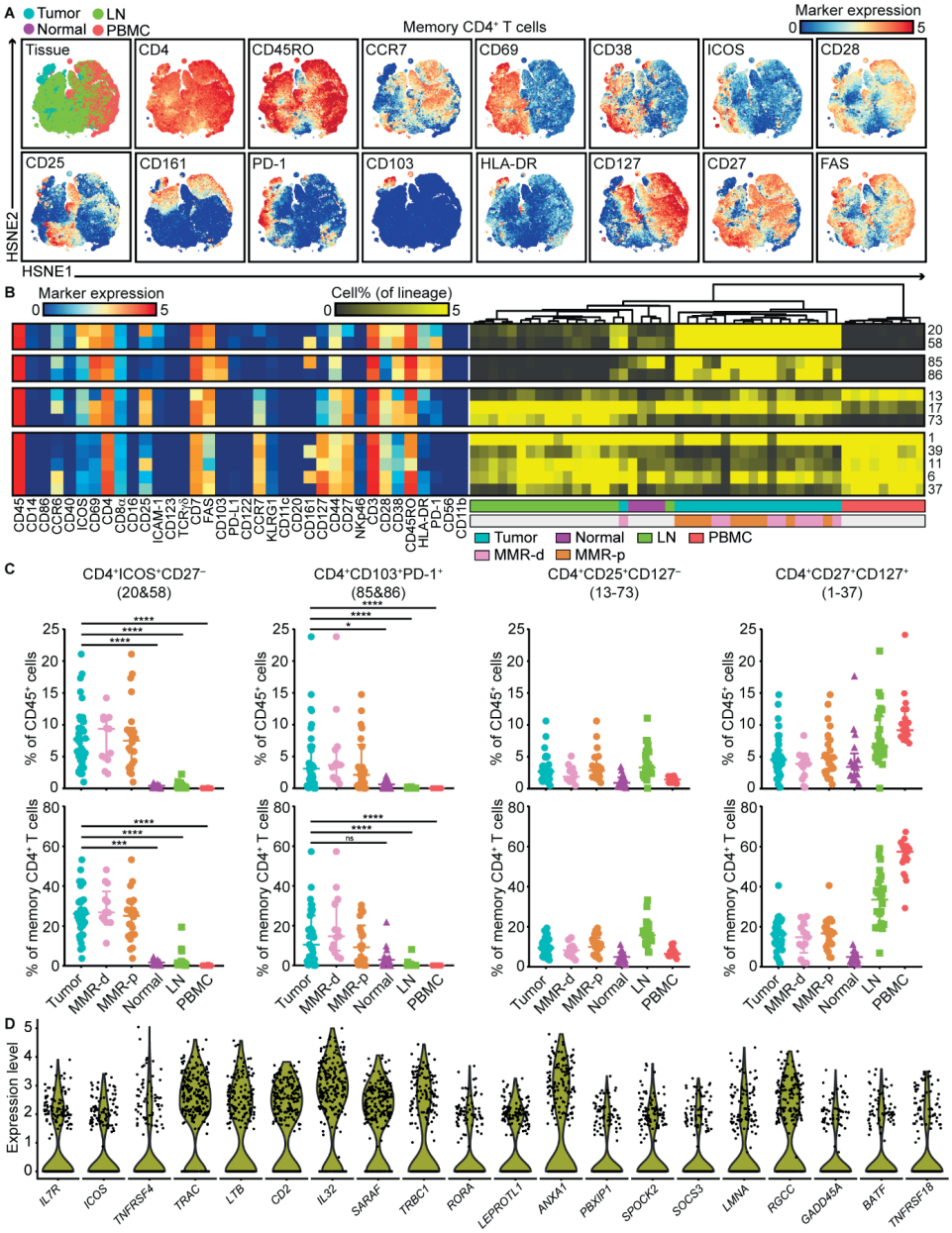

Figure 3. ICOS⁺ and activated CD4⁺ T cells are dominant, tumor tissue-specific T cell populations in both mismatch repair-deficient and -proficient colorectal cancers.

A. HSNE embedding of $3.1*10^5$ landmarks representing the memory CD4⁺ T cell compartment ($2.0*10^6$ cells) from the discovery cohort of CRC patients colored by tissue type (first plot) and relative expression of indicated markers. **B.** A heatmap showing median marker expression values (left) and a heatmap showing frequencies of selected memory CD4⁺ T cell clusters (right). Hierarchical clustering was performed on cluster frequencies using Spearman's rank correlation. Color bars indicate tissue type. **C.** Frequencies of selected memory CD4⁺ T cell clusters among CRC patients' tissues (N=35, further subdivided into MMR-deficient (N=13) and MMR-proficient (N=22)), colorectal healthy mucosa (N=17), tumor-associated lymph nodes (N=26), and peripheral blood (N=19) as percentage of total CD45⁺ cells

(upper panel) and memory CD4⁺ T cells (lower panel). Cluster IDs correspond to the ones in (**B**). Bars indicate median ± IQR. Each dot represents an individual sample. Data from 22 independent experiments with mass cytometry. *P<0.05, ***P<0.001, ****P<0.0001 by Kruskal-Wallis test with Dunn's test for multiple comparisons. **D.** Violin plot showing log-transformed expression levels of the top 20 differentially expressed genes within CD4⁺ T cells (N=245) analyzed by single-cell RNA-sequencing on CD45⁺ cells from 7 tumors (**Figure 1D**). Each dot represents a single cell.

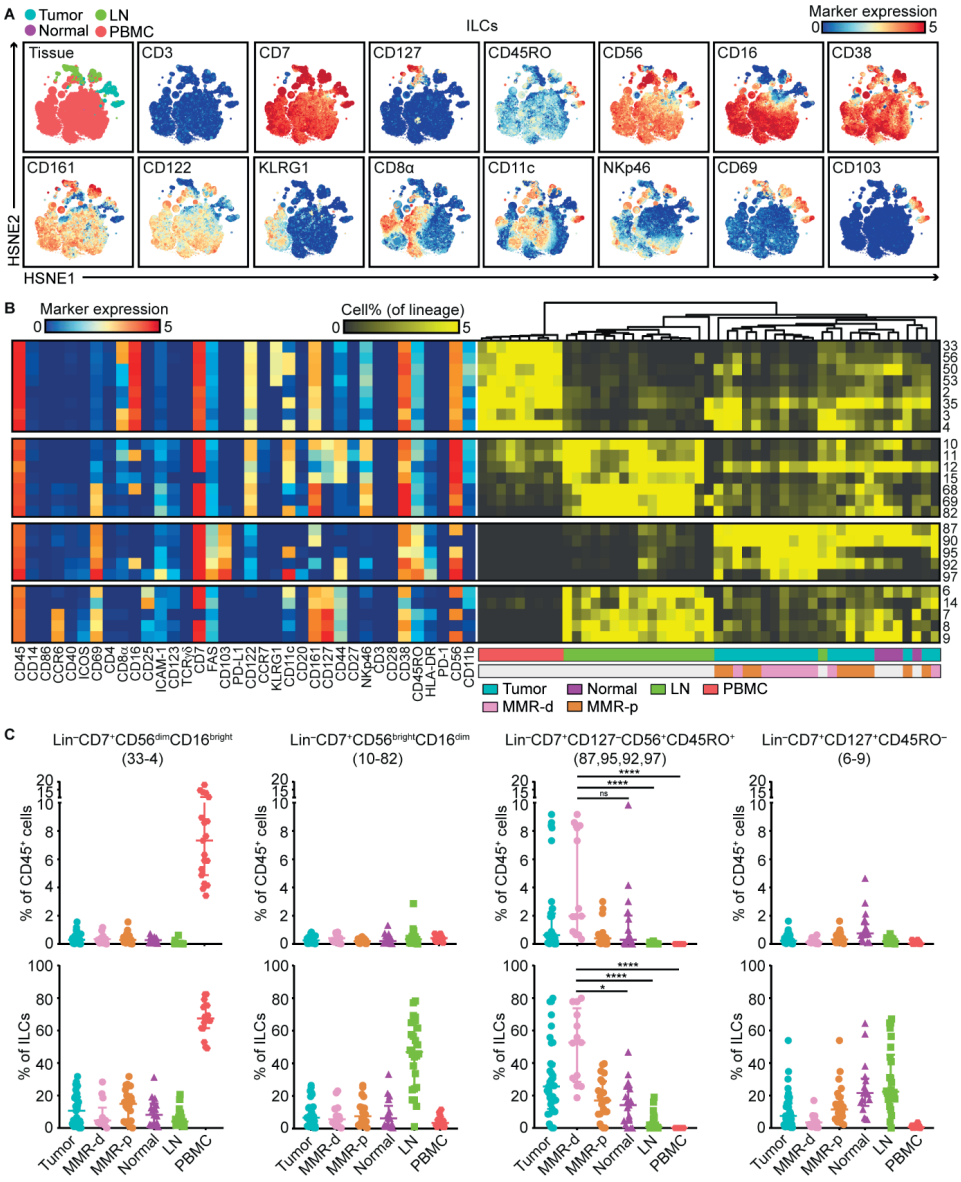

Figure 4. CD127⁻CD56⁺CD45RO⁺ ILCs are the prevalent ILC population in mismatch repair-deficient colorectal tumors.

A. HSNE embedding of 5.5*10⁴ landmarks representing the innate lymphoid compartment (0.4*10⁶ cells) from the discovery cohort of CRC patients colored by tissue type (first plot) and relative expression of indicated markers. **B.** A heatmap showing median marker expression values (left) and a heatmap showing frequencies of selected ILC

clusters (right). Hierarchical clustering was performed on cluster frequencies using Spearman's rank correlation. Color bars indicate tissue type. **C.** Frequencies of selected innate lymphoid clusters among CRC patients' tissues (N=35, further subdivided into MMR-deficient (N=13) and MMR-proficient (N=22)), colorectal healthy mucosa (N=17), tumor-associated lymph nodes (N=26), and peripheral blood (N=19) as percentage of total CD45$^+$ cells (upper panel) and ILCs (lower panel). Cluster IDs correspond to the ones in (**B**). Bars indicate median ± IQR. Each dot represents an individual sample. Data from 22 independent experiments with mass cytometry. NS, not significant, *P<0.05, ****P<0.0001 by Kruskal-Wallis test with Dunn's test for multiple comparisons.

Tumor-resident ILCs are involved in the anti-tumor immune response

Single-cell RNA-sequencing unveiled high expression levels of cytotoxic molecules (e.g. *GNLY*, *PRF1*, *GZMA*, *GZMB*) in the ILC cluster (**Figure 5A**). In addition, we observed the presence of transcripts for a member of the killer-cell immunoglobulin-like receptor (KIR) family, *KIR2DL4* (**Figure 5A**). We performed additional single-cell RNA-sequencing on CD45$^+$ cells from one MMR-deficient tumor with high numbers of Lin$^-$CD7$^+$CD127$^-$CD56$^+$CD45RO$^+$ ILCs (70% of the ILC cluster), as revealed by mass cytometry data. Here, we also observed high expression levels of cytotoxic molecules (e.g. *GNLY*, *PRF1*, *GZMA*) as well as the expression of *KIR2DL4* and *KIR3DL2* in the ILC cluster (**Figure S7**). Cell surface expression of KIRs was confirmed by flow cytometry in Lin$^-$CD7$^+$CD127$^-$CD56$^+$CD45RO$^+$ ILCs from this tumor (**Figure S7**).

To further investigate functional properties of tumor-resident lymphocytes, we designed a flow cytometry antibody panel to analyze the cytotoxic potential of Lin$^-$CD7$^+$CD127$^-$CD56$^+$CD45RO$^+$ ILCs, Lin$^-$CD7$^+$CD127$^-$CD56$^+$CD45RA$^+$ NK cells, and memory CD8$^+$ T cells in CRC tissues (**Table S3**). Strikingly, up to 82.3% of unstimulated CD127$^-$CD56$^+$CD45RO$^+$ ILCs displayed granzyme B/perforin expression in the tumor tissues (**Figure 5B**). Granzyme B/perforin expression by the ILCs was most abundant in MMR-deficient cancers as compared to MMR-proficient cancers (**Figure 5C**). Interestingly, the cytotoxic capacity of CD127$^-$CD56$^+$CD45RO$^+$ ILCs was accompanied by similar profiles in CD127$^-$CD56$^+$CD45RA$^+$ NK cells and memory CD8$^+$ T cells across samples (**Figure 5C**), suggesting a coordinated cytotoxic innate and adaptive immune response in CRC tissues.

To investigate the spatial localization of the ILCs in CRCs, we applied 6-color multispectral immunofluorescence to frozen tissue sections of 4 MMR-deficient and 4 MMR-proficient CRCs (**Table S4**). We simultaneously detected CD3, TCRαβ, CD127, CD7, CD45RO, and DAPI. We identified CD3$^-$TCRαβ$^-$CD127$^-$CD7$^+$CD45RO$^+$ ILCs in the tumors (**Figure 6A,B**), and observed an increased presence of these cells in MMR-deficient as compared to MMR-proficient CRCs (**Figure 6C**). Interestingly, the CD3$^-$TCRαβ$^-$CD127$^-$CD7$^+$CD45RO$^+$ ILCs frequently displayed an intraepithelial localization in agreement with their CD103$^+$CD69$^+$ tissue-resident phenotype (**Figure 6A**).

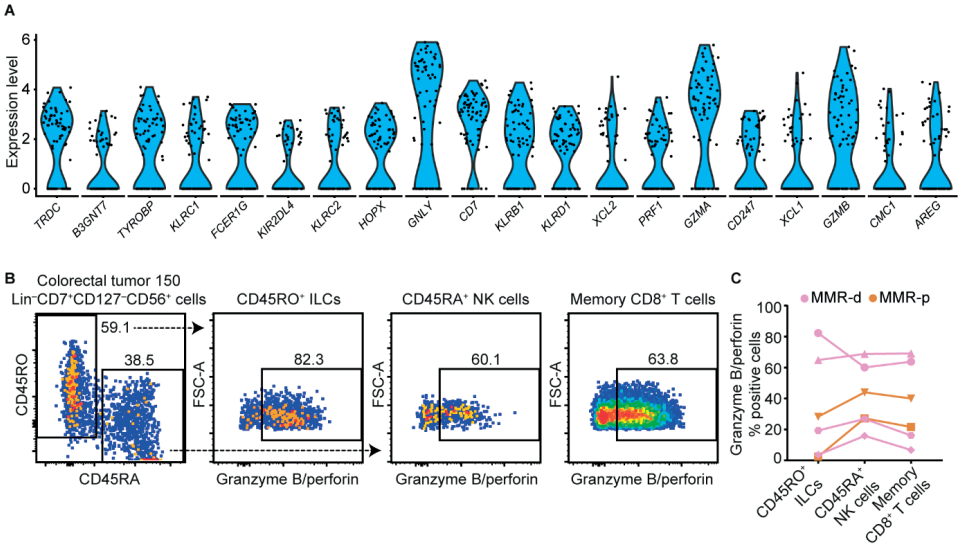

Figure 5. Tumor-resident ILCs are involved in the anti-tumor immune response.
A. Violin plot showing log-transformed expression levels of the top 20 differentially expressed genes within ILCs (N=74) analyzed by single-cell RNA-sequencing on CD45$^+$ cells from 7 tumors (**Figure 1D**). Each dot represents a single cell. **B.** Representative plots of a MMR-deficient tumor sample analyzed by flow cytometry without stimulation showing the distinction between CD45RO$^+$ ILCs and CD45RA$^+$ NK cells within Lin$^-$CD7$^+$CD127$^-$CD56$^+$ cells (first plot), and their expression of cytotoxic molecules. **C.** Granzyme B/perforin expression in different immune cell populations of CRC tissues (N=6, of which 4 MMR-deficient and 2 MMR-proficient). Dot shape indicates similar tumor samples. Data from three independent experiments with flow cytometry.

Immune-system-wide analysis reveals correlations between innate and adaptive immune cell subsets in colorectal cancer

Lastly, we integrated the identified immune cell clusters across all major immune lineages (N=218) in one immune-system-wide analysis to characterize the samples according to tissue type, MMR status, and available clinico-pathological parameters. The integrated t-SNE analysis confirmed the unique immune composition in the different tissue types, and visualized the top ten ranked immune cell clusters contributing to the distinctive clustering patterns of the samples (**Figure S8**). No association was observed with clinical stage while differences related to tumor location and HLA class I expression can be attributed to features that distinguish MMR-deficient and -proficient CRCs (**Figure S8**).

Spearman's rank correlation analysis performed on the top ten ranked unique immune cell clusters of each tissue type revealed strong correlations between the presence of CD127$^-$CD56$^+$CD45RO$^+$ ILCs (ILC97,92,95) and the presence of CD103$^+$PD-1$^+$ cytotoxic (CD8memory60,96), helper (CD4memory85,86), and γδ (TCR γδ99) T cell populations in MMR-deficient CRCs (**Figure 7**, **Table S5**). In contrast, MMR-proficient tumors were characterized by the presence of several myeloid populations (**Figure 7**, **Table S5**).

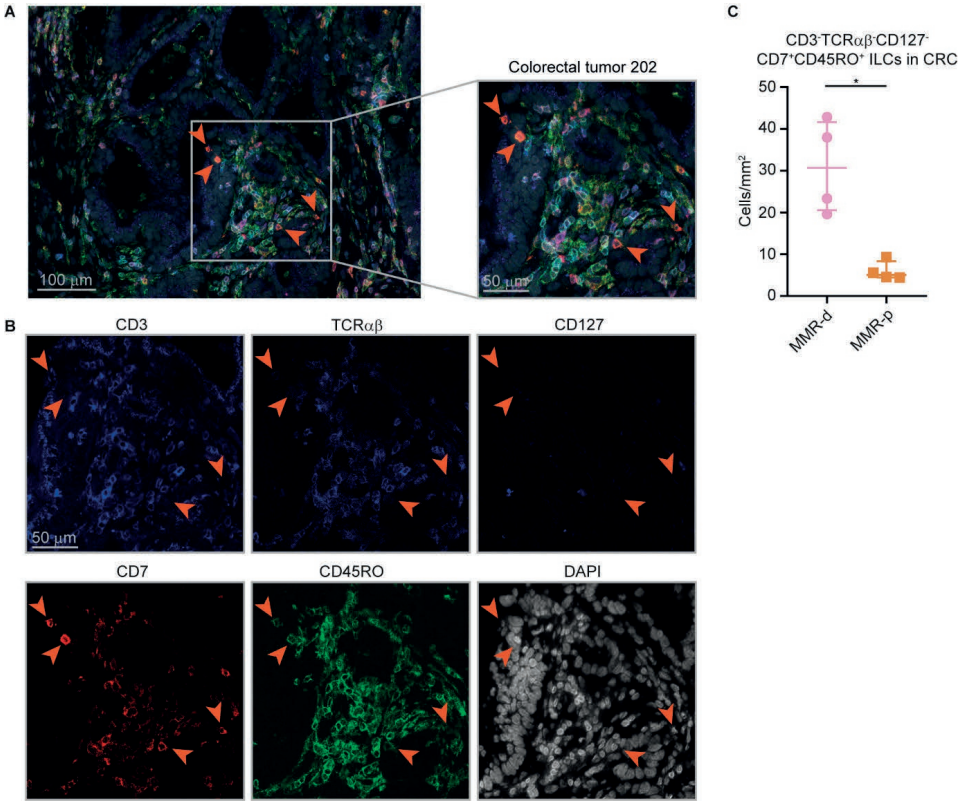

Figure 6. Higher cell density of CD127⁻CD45RO⁺ ILCs in mismatch repair-deficient colorectal cancers.
A and B. Representative image of the immunofluorescence microscopic detection of CD3⁻TCRαβ⁻CD127⁻CD7⁺CD45RO⁺ ILCs in a MMR-deficient tumor, showing CD3 (colored in blue), TCRαβ (colored in blue), CD127 (colored in blue), CD7 (colored in red), CD45RO (colored in green), and DAPI (colored in grey) as nuclear counterstain. **C.** Frequencies of CD3⁻TCRαβ⁻CD127⁻CD7⁺CD45RO⁺ ILCs in 4 MMR-deficient and 4 MMR-proficient CRCs. *P<0.05 by Mann-Whitney U test.

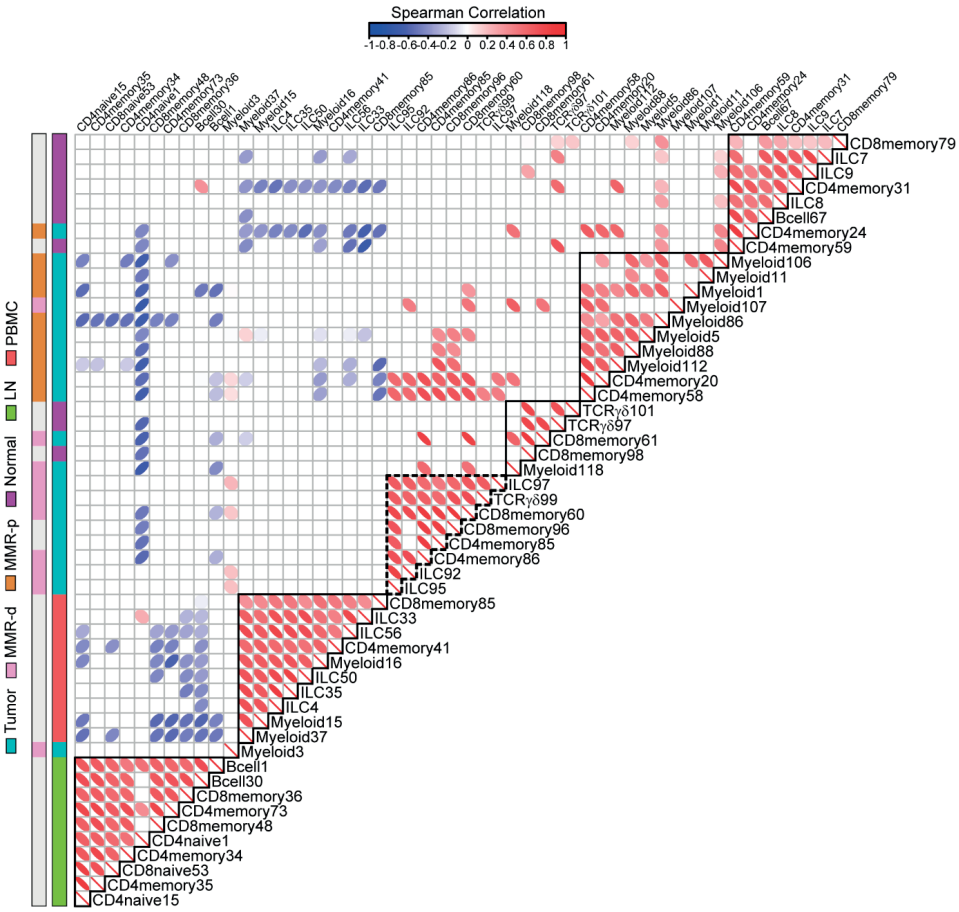

Figure 7. Immune-system-wide analysis reveals correlations between innate and adaptive immune cell subsets in colorectal cancer.

Matrix showing correlations (Spearman's ρ, see **Supplemental methods**) between unique top ten ranked immune cell clusters for each tissue type (shown in **Figure S8**) based on cell percentages (of total CD45$^+$ cells) corresponding to 97 samples from 31 CRC patients. Color and shape of the ellipses in the heatmap indicate the strength of the correlation. Only significant correlation coefficients are shown. Color bars indicate tissue type. Coefficient and *P*-values of correlations for CRC tissues are shown in **Table S5**. *P*-values were adjusted for multiple testing using the Benjamini-Hochberg procedure. Data from 22 independent experiments with mass cytometry.

DISCUSSION

We applied mass cytometry to comprehensively analyze the immune landscape of CRCs at single-cell level in tumor and healthy tissues. Our analysis revealed tumor tissue-specific immune signatures across the innate and adaptive immune compartments of CRC. Immunohistochemistry, flow cytometry, and recent transcriptomic approaches have provided insight into the complexity of tumor immune landscapes.[15-19] However, the number of markers that can be simultaneously assayed in immunohistochemistry or flow cytometry is limited, and bulk transcriptomic studies do not allow for discrimination of phenotypes at

the cellular level.[20,21] In mass cytometry over 40 markers can be simultaneously analyzed at single-cell level, providing a unique opportunity to obtain a comprehensive overview of tumor-resident lymphocytes.[22,23] Here, we combined mass cytometry phenotypes with functional, transcriptional, and spatial analyses of tumor-resident immune cell populations in CRC.

Within the innate compartment, we observed that a previously unappreciated innate lymphoid population, Lin$^-$CD7$^+$CD127$^-$CD56$^+$CD45RO$^+$ ILCs, is enriched in MMR-deficient tumors and displayed cytotoxic activity. *In-situ* detection of the ILCs confirmed a higher cell density in MMR-deficient CRCs, and showed a frequent intraepithelial localization. This is in line with their tissue-resident phenotype (CD103$^+$CD69$^+$), and supports an active role for these cells in the anti-tumor immune response. The ILCs resemble previous descriptions of TCR$^-$CD103$^+$ cells in mice that were found to express granzyme B.[24] Additionally, a unique subset of NK cells has been found in several human tissues and was described as NKp44$^+$CD103$^+$ intraepithelial ILC1-like.[25,26] In contrast to NKp44$^+$CD103$^+$ ILC1, the CD127$^-$CD56$^+$CD45RO$^+$ ILCs identified here lacked CD122 and NKp46 expression (**Figure 4B**), and showed low levels of NKp44 (data not shown). These variable marker expression patterns most likely represent additional levels of plasticity and heterogeneity within ILC subsets. Single-cell RNA-sequencing revealed the presence of transcripts for *KIR2DL4* and *KIR3DL2* in the ILC cluster, which hints toward potential activation mechanisms.[27] Common ligands of KIRs include HLA class I molecules,[28,29] and loss of HLA class I expression has been described to occur in the majority of MMR-deficient CRCs.[30-32] It is tempting to speculate that CD127$^-$CD56$^+$CD45RO$^+$ ILC-mediated cytotoxicity toward such HLA-loss variants may contribute to the anti-tumor response in MMR-deficient CRCs, a link that requires further investigation.

The presence of CD127$^-$CD56$^+$CD45RO$^+$ ILCs strongly correlated with tissue-resident CD103$^+$CD69$^+$ γδ T cells co-expressing activation markers HLA-DR, CD38, and PD-1 in MMR-deficient CRCs. It has been shown that human peripheral blood γδ T cells can express PD-1 and exhibit natural killer-like activity.[33] The expression of PD-1, in conjunction with their cytotoxic potential, suggest an active role of tumor-resident γδ T cells in the anti-tumor immune response and potentially as targets for PD-1 checkpoint blockade. This will be subject of further studies.

Within the adaptive compartment, we found dominant, tumor tissue-specific CD8$^+$ and CD4$^+$ T cell populations that displayed a highly similar activated tissue-resident phenotype. Such CD8$^+$ T cell populations have been described in ovarian cancer,[34,35] lung cancer,[36] and recently in melanoma,[37] cervical carcinoma[38] and CRC,[12,13] and their presence was associated with an improved clinical prognosis. Single-cell RNA-sequencing revealed that CD8$^+$ T cells in colorectal tumors showed a cytotoxic profile, indicative of potential anti-tumor reactivity. In addition, we found a dominant tumor tissue-specific population of ICOS$^+$ CD4$^+$ T cells. ICOS belongs to the CD28/CTLA-4 family and serves as a co-stimulatory molecule for T cell activation.[39] Activation of ICOS by agonists has been proposed for anti-cancer treatment.[40] Here, we identified a CD161$^+$PD-1$^+$ as well as a CD25$^+$ population of tumor-resident ICOS$^+$ CD4$^+$ T cells. The latter corresponds to a regulatory T cell subset displaying high levels of

FOXP3 expression, that, interestingly, expressed higher levels of ICOS as compared to the CD161^{+}PD-1^{+} counterpart. The use of ICOS agonists may, therefore, also result in activation of ICOS^{+} T cells with suppressive and regulatory properties in the tumor microenvironment. In contrast to the tumor-resident CD8^{+} T cells, ICOS^{+} CD4^{+} T cells were present in both MMR-deficient and MMR-proficient tumors to a similar extent.

We observed CD161^{+} and CD161^{-} counterparts of tumor-resident cytotoxic and helper T cells, and CD127^{-}CD56^{+}CD45RO^{+} ILCs. CD161 has been shown to mark a subset of tissue-resident memory CD8^{+} T cells with enhanced effector function and cytokine production.[41,42] In our study, the CD161^{-} counterpart of the tumor-resident T cell and ILC populations was particularly enriched in MMR-deficient CRCs as compared to MMR-proficient CRCs. The functional relevance of this observation will be subject of future studies. Nevertheless, we observed increased CD161 expression in PD-1 high cells as compared to PD-1 intermediate/negative cells for tumor-resident CD8^{+} and CD4^{+} T cell populations (**Figure S9**). As PD-1 high cells in human cancer have been associated with a state of T cell dysfunction,[43-45] CD161 expression could be an additional marker for this functional state.

Interestingly, we identified what could be the non-activated counterparts of the CD103^{+}PD-1^{+} cytotoxic and γδ T cells in both tumor and healthy colorectal tissues. Mobilization and activation of these cells from the colorectal healthy mucosa to the tumor tissue may be beneficial for immunotherapy in CRC. Strikingly, while lymph nodes are traditionally viewed as key players of anti-tumor immune responses, we did not detect non-activated precursors of tumor-resident immune cell populations in the lymph node samples, with the exception of tumor-positive lymph nodes. Furthermore, we observed that lymph nodes harboured a large population of CD4^{+}CD25^{+}CD127^{-} Tregs, suggesting they might be a primary source of Tregs in the cancer microenvironment. The tumor-resident immune cell populations were also not mirrored in peripheral blood, although the in-depth investigation of their presence in these tissues with complementary approaches should be conducted.

It should be noted that the mass cytometry antibody panel was primarily developed to characterize T cell, γδ T cell and ILC compartments, and in future studies additional efforts are required to further explore the myeloid and B cell compartment. Furthermore, the number and pattern of infiltrating lymphocytes can be influenced by various tumor characteristics. In this study we have shown profound differences in lymphocytic infiltration that distinguish MMR-deficient from MMR-proficient CRCs. Other factors not investigated in this study that can influence the infiltration of lymphocytes in tumors include for instance occurrence of somatic mutations (neoantigens) and the co-occurrence of inflammatory bowel disease. Although the results are of preliminary nature, they point to the involvement of additional subsets than T cells in immune responses to CRC, particularly ILCs and γδ T cells. This is especially relevant in the context of responses to checkpoint blockade therapy in absence of HLA class I expression.[46] Future approaches might opt for an in-depth investigation of these specific lineages for a detailed characterization of phenotypes that complement the markers used in this study. The next step will be to investigate the involvement of these subsets in

the clinical setting of patients treated by checkpoint blockade.

In conclusion, we identified a previously unappreciated innate immune cell population that was specifically enriched in CRC tissues, displayed cytotoxic activity, and strongly contributed to a data-driven distinction between immunogenic (MMR-deficient) and non-immunogenic (MMR-proficient) tumors. Furthermore, we revealed strong correlations between the presence of these innate cells and tumor-resident $CD8^+$, $CD4^+$, and $\gamma\delta$ T cells with an activated phenotype in MMR-deficient tumors that together may play a critical role in tumor control.

METHODS

Human samples

Primary CRC tissues (N=35, of which 22 MMR-proficient and 13 MMR-deficient) with matched tumor-associated lymph nodes (N=26), colorectal healthy mucosa (N=17), and pre-surgical peripheral blood samples (N=19) from 31 CRC patients were processed for this study (**Table S1**). All patients were treatment-naïve except five rectal cancer patients which received neo-adjuvant therapy (**Table S1**). One patient was diagnosed with multiple primary colorectal tumors (N=5) at different locations, all of which were included in the study (**Table S1**). No patient with a previous history of inflammatory bowel disease was studied. To account for tumor heterogeneity, macroscopic sectioning from the lumen to the most invasive area of the tumor was performed for further processing. This study was approved by the Medical Ethical Committee of the Leiden University Medical Center (protocol P15.282), and patients provided written informed consent. All specimens were anonymized and handled according to the ethical guidelines described in the Code for Proper Secondary Use of Human Tissue in the Netherlands of the Dutch Federation of Medical Scientific Societies.

Tissue processing and mass cytometry antibody staining

Details on tissue processing and mass cytometry antibody staining are available in **Supplemental methods** and **Table S2**.

Mass cytometry data analysis

Mass cytometry experiments were performed with a discovery and validation cohort of CRC patients. The discovery cohort consisted of 19 CRC tissues, 17 tumor-associated lymph nodes, 4 colorectal healthy mucosa, and 9 peripheral blood samples. Single, live $CD45^+$ cells were gated in Cytobank[47] (**Figure S1**). $CD45^+$ cells were sample-tagged, hyperbolic ArcSinh transformed with a cofactor of 5, and subjected to dimensionality reduction analysis in Cytosplore.[48] Of the 39 antibodies included in the panel, 36 showed clear discrimination between positive and negative cells (**Figure S1**). Major immune lineages (**Figure 1A,B**) were identified at the overview level of a 5-level Hierarchical Stochastic Neighbor Embedding (HSNE) analysis[49,50] on $CD45^+$ data from all samples ($8.9*10^6$ cells) with default perplexity and iterations (30 and 1,000, respectively). Naive and memory $CD4^+$ and $CD8^+/\gamma\delta$ T cell, B cell, Lin^-CD7^+ innate lymphoid cell (ILC), and myeloid cell lineages were analyzed in a data-driven manner up to a maximum number of $0.5*10^6$ landmarks.[50] Clustering of the data was performed by Gaussian Mean Shift (GMS) clustering in Cytosplore, and an algorithm was run that merged clusters showing high similarity in ArcSinh5-transformed median expression of all markers (<1). Hierarchical clustering on cell frequencies was performed in Matlab using Spearman's rank correlation.

The validation cohort consisted of 16 CRC tissues, 9 tumor-associated lymph nodes, 13 colorectal healthy mucosa, and 10 peripheral blood samples. Single, live $CD45^+$ cells were hyperbolic ArcSinh transformed with a cofactor of 5, and classified into the pre-identified immune cell clusters of the discovery cohort based on similarity in marker expression. To obtain consistent cell clusters across both cohorts, a Linear Discriminant Analysis classifier was trained using the cell clusters of the discovery cohort and was used to automatically predict the cluster label for each cell in the validation cohort.[51] To account for technical variation, a peripheral blood mononuclear cell (PBMC) reference sample was included in every mass cytometry experiment. ComBat was applied to align the PBMC reference samples and corresponding patient samples to correct for batch effects.[52]

Single-cell RNA-sequencing

$CD45^+$ cells from 7 tumors (4 MMR-deficient and 3 MMR-proficient) were MACS-sorted with anti-CD45-PE antibodies (clone 2D1, Thermo Fisher Scientific) and anti-PE microbeads (Miltenyi Biotec). Single-cell RNA-sequencing libraries were prepared using the Chromium Single Cell 3' Reagent Kit, Version 2

Chemistry (10x Genomics) according to the manufacturer's protocol. Libraries were sequenced on a NovaSeq6000 using paired-end 2x150bp sequencing (Illumina). Downstream analysis was performed using the Seurat R package according to the author's instructions.[53] Briefly, cells with fewer than 200 expressed genes, and genes that were expressed in less than 3 cells were excluded. Furthermore, cells with outlying percentages of differentially expressed mitochondrial genes (>0.20) and cells with outlying numbers of expressed genes (>5000) were excluded. This resulted in a final dataset of 1,079 cells expressing a total of 1,972 variable genes. Cells were pre-processed using principal component analysis, clustered using graph-based community detection,[54] and visualized by t-distributed Stochastic Neighbor Embedding (t-SNE)[55]. Differentially expressed genes were identified for each cell cluster and visualized in violin plots. In addition, CD45$^+$ cells from one MMR-deficient tumor with high numbers of Lin$^-$CD7$^+$CD127$^-$CD56$^+$CD45RO$^+$ ILCs were sorted on a FACS Aria II sorter (BD Biosciences) (**Table S3**). A similar single-cell RNA-sequencing analysis pipeline was performed while sequencing was performed on a HiSeq4000 (Illumina). Cut-offs for outlying percentages of differentially expressed mitochondrial genes (>0.05) and cells with outlying numbers of expressed genes (>5500) were used. Here, a final dataset of 795 cells expressing a total of 1,814 variable genes was obtained.

Flow cytometry

Single-cell suspensions of CRC tissues (N=8, of which 5 MMR-deficient and 3 MMR-proficient) were stimulated in IMDM/L-glutamine medium (Lonza) complemented with 10% human serum with 20 ng/mL PMA (Sigma-Aldrich) and 1 µg/mL ionomycin (Sigma-Alrdich) for 6 hr at 37°C. Ten µg/mL brefeldin A (Sigma-Aldrich) was added for the last 4 hours. A flow cytometry antibody panel was designed to detect granzyme B/perforin, IFN-γ, and TNF-α production by ILC, T cell, and γδ T cell populations (**Table S3**). In addition, FOXP3 expression by ICOS$^+$ regulatory T cells was assessed in single-cell suspensions of CRC tissues (N=4, of which 1 MMR-deficient and 3 MMR-proficient). Details on flow cytometry antibody staining are available in **Supplemental methods**.

Immunohistochemical staining

Details on immunohistochemical detection of MMR proteins and human leukocyte antigen (HLA) class I expression of CRC tissues are available in **Supplemental methods**.

Multispectral immunofluorescence

A six-marker immunofluorescence panel was applied to 5-µm frozen tissue sections of 4 MMR-deficient and 4 MMR-proficient colorectal tumors, as described previously[56]. Details on immunofluorescence antibody staining are available in **Supplemental methods** and **Table S4**. For each tumor, five different tissue sections were imaged at 20x magnification with the Vectra 3.0 Automated Quantitative Pathology Imaging System (Perkin Elmer). InForm Cell Analysis software (Perkin Elmer) was used for image analysis and spectral separation of dyes, by using spectral libraries defined with single-marker immunofluorescence detection. Tissue segmentation was trained manually with DAPI to segment images into tissue and 'no tissue' areas. All images were visually inspected for the number of CD3$^-$TCRαβ$^-$CD127$^-$CD7$^+$CD45RO$^+$ ILCs and cell counts were normalized by tissue area (number of cells per mm^2).

Statistical analysis

Data were presented as median ± interquartile range. Group comparisons were performed with Mann-Whitney U test, Kruskal-Wallis test with Dunn's test for multiple comparisons, or Friedman test with Dunn's test for multiple comparisons (GraphPad Prism version 7), as indicated. In the correlation analysis, *P*-values were adjusted for multiple testing using the Benjamini-Hochberg procedure. *P*-values < 0.05 were considered statistically significant.

ACKNOWLEDGEMENTS

We thank M.G. Kallenberg-Lantrua, A.M.E.G. Voet-van den Brink, and F.A. Holman for their help in collecting and providing samples from CRC patients; J. van den Bulk for the isolation of PBMCs from

CRC patients; W.E. Corver for flow cytometric cell sorting, R.J. McLaughlin for providing help with mass cytometry experiments, the Leiden Genome Technology Center for their help with single-cell RNA-sequencing, and J. Oosting for help with statistical analysis.

AUTHOR CONTRIBUTIONS

N.L. de Vries conceived the study, performed experiments, and wrote the manuscript. N.L. de Vries, V. van Unen, M.E. Ijsselsteijn, T. Abdelaal, and A. Mahfouz analyzed the data. A. Farina Sarasqueta and K.C.M.J. Peeters provided samples from patients. M.E. Ijsselsteijn, R. van der Breggen, and N.F. de Miranda processed the samples and performed experiments. T. Höllt, V. van Unen, and B.P.F. Lelieveldt developed Cytosplore and HSNE applications. F. Koning and N.F. de Miranda initiated and led the project, and wrote the manuscript. All authors discussed the results and commented on the manuscript.

COMPETING INTERESTS

None to declare.

REFERENCES

1 Hodi, F. S. *et al.* Improved survival with ipilimumab in patients with metastatic melanoma. *N Engl J Med* 363, 711-723, doi:10.1056/NEJMoa1003466 (2010).

2 Topalian, S. L. *et al.* Safety, activity, and immune correlates of anti-PD-1 antibody in cancer. *N Engl J Med* 366, 2443-2454, doi:10.1056/NEJMoa1200690 (2012).

3 Rizvi, N. A. *et al.* Cancer immunology. Mutational landscape determines sensitivity to PD-1 blockade in non-small cell lung cancer. *Science* 348, 124-128, doi:10.1126/science.aaa1348 (2015).

4 Kelderman, S., Schumacher, T. N. & Kvistborg, P. Mismatch Repair-Deficient Cancers Are Targets for Anti-PD-1 Therapy. *Cancer Cell* 28, 11-13, doi:10.1016/j.ccell.2015.06.012 (2015).

5 Le, D. T. *et al.* Mismatch repair deficiency predicts response of solid tumors to PD-1 blockade. *Science* 357, 409-413, doi:10.1126/science.aan6733 (2017).

6 Ionov, Y., Peinado, M. A., Malkhosyan, S., Shibata, D. & Perucho, M. Ubiquitous somatic mutations in simple repeated sequences reveal a new mechanism for colonic carcinogenesis. *Nature* 363, 558-561, doi:10.1038/363558a0 (1993).

7 Comprehensive molecular characterization of human colon and rectal cancer. *Nature* 487, 330-337, doi:10.1038/nature11252 (2012).

8 Smyrk, T. C., Watson, P., Kaul, K. & Lynch, H. T. Tumor-infiltrating lymphocytes are a marker for microsatellite instability in colorectal carcinoma. *Cancer* 91, 2417-2422 (2001).

9 de Miranda, N. F. *et al.* Infiltration of Lynch colorectal cancers by activated immune cells associates with early staging of the primary tumor and absence of lymph node metastases. *Clin Cancer Res* 18, 1237-1245, doi:10.1158/1078-0432.CCR-11-1997 (2012).

10 Chevrier, S. *et al.* An Immune Atlas of Clear Cell Renal Cell Carcinoma. *Cell* 169, 736-749 e718, doi:10.1016/j.cell.2017.04.016 (2017).

11 Zheng, C. *et al.* Landscape of Infiltrating T Cells in Liver Cancer Revealed by Single-Cell Sequencing. *Cell* 169, 1342-1356 e1316, doi:10.1016/j.cell.2017.05.035 (2017).

12 Duhen, T. *et al.* Co-expression of CD39 and CD103 identifies tumor-reactive CD8 T cells in human solid tumors. *Nat Commun* 9, 2724, doi:10.1038/s41467-018-05072-0 (2018).

13 Simoni, Y. *et al.* Bystander CD8(+) T cells are abundant and phenotypically distinct in human tumor infiltrates. *Nature* 557, 575-579, doi:10.1038/s41586-018-0130-2 (2018).

14 Li, N. *et al.* Mass cytometry reveals innate lymphoid cell differentiation pathways in the human fetal intestine. *J Exp Med*, doi:10.1084/jem.20171934 (2018).

15 Menon, A. G. *et al.* Immune system and prognosis in colorectal cancer: a detailed immunohistochemical analysis. *Lab Invest* 84, 493-501, doi:10.1038/labinvest.3700055 (2004).

16 Galon, J. *et al.* Type, density, and location of immune cells within human colorectal tumors predict clinical outcome. *Science* 313, 1960-1964, doi:10.1126/science.1129139 (2006).

17 Angelova, M. *et al.* Characterization of the immunophenotypes and antigenomes of colorectal cancers reveals distinct tumor escape mechanisms and novel targets for immunotherapy. *Genome Biol* 16, 64, doi:10.1186/s13059-015-0620-6 (2015).

18 Guinney, J. *et al.* The consensus molecular subtypes of colorectal cancer. *Nat Med* 21, 1350-1356, doi:10.1038/nm.3967 (2015).

19 Li, H. *et al.* Reference component analysis of single-cell transcriptomes elucidates cellular heterogeneity in human colorectal tumors. *Nat Genet* 49, 708-718, doi:10.1038/ng.3818 (2017).

20 Peterson, V. M. *et al.* Multiplexed quantification of proteins and transcripts in single cells. *Nat Biotechnol*, doi:10.1038/nbt.3973 (2017).

21 Schulz, D. *et al.* Simultaneous Multiplexed Imaging of mRNA and Proteins with Subcellular Resolution in Breast Cancer Tissue Samples by Mass Cytometry. *Cell Syst* 6, 25-36 e25, doi:10.1016/j.cels.2017.12.001 (2018).

22 Bandura, D. R. *et al.* Mass cytometry: technique for real time single cell multitarget immunoassay based on inductively coupled plasma time-of-flight mass spectrometry. *Anal Chem* 81, 6813-6822, doi:10.1021/ac901049w (2009).

23 Bendall, S. C., Nolan, G. P., Roederer, M. & Chattopadhyay, P. K. A deep profiler's guide to cytometry. *Trends in immunology* 33, 323-332, doi:10.1016/j.it.2012.02.010 (2012).

24 Dadi, S. *et al.* Cancer Immunosurveillance by Tissue-Resident Innate Lymphoid Cells and Innate-like T Cells. *Cell* 164, 365-377, doi:10.1016/j.cell.2016.01.002 (2016).

25 Fuchs, A. *et al.* Intraepithelial type 1 innate lymphoid cells are a unique subset of IL-12- and IL-15-responsive IFN-gamma-producing cells. *Immunity* 38, 769-781, doi:10.1016/j.immuni.2013.02.010 (2013).

26 Simoni, Y. *et al.* Human Innate Lymphoid Cell Subsets Possess Tissue-Type Based Heterogeneity in Phenotype and Frequency. *Immunity* 46, 148-161, doi:10.1016/j.immuni.2016.11.005 (2017).

27 Wagtmann, N. *et al.* Molecular clones of the p58 NK cell receptor reveal immunoglobulin-related molecules with diversity in both the extra- and intracellular domains. *Immunity* 2, 439-449 (1995).

28 Rajagopalan, S. & Long, E. O. KIR2DL4 (CD158d): An activation receptor for HLA-G. *Front Immunol* 3, 258, doi:10.3389/fimmu.2012.00258 (2012).

29 Moretta, A. *et al.* P58 molecules as putative receptors for major histocompatibility complex (MHC) class I molecules in human natural killer (NK) cells. Anti-p58 antibodies reconstitute lysis of MHC class I-protected cells in NK clones displaying different specificities. *J Exp Med* 178, 597-604 (1993).

30 Dierssen, J. W. *et al.* HNPCC versus sporadic microsatellite-unstable colon cancers follow different routes toward loss of HLA class I expression. *BMC Cancer* 7, 33, doi:10.1186/1471-2407-7-33 (2007).

31 Kloor, M. *et al.* Immunoselective pressure and human leukocyte antigen class I antigen machinery defects in microsatellite unstable colorectal cancers. *Cancer Res* 65, 6418-6424, doi:10.1158/0008-5472.can-05-0044 (2005).

32 Ijsselsteijn, M. E. *et al.* Revisiting immune escape in colorectal cancer in the era of immunotherapy. *Br J Cancer* 120, 815-818, doi:10.1038/s41416-019-0421-x (2019).

33 Iwasaki, M. *et al.* Expression and function of PD-1 in human gammadelta T cells that recognize phosphoantigens. *Eur J Immunol* 41, 345-355, doi:10.1002/eji.201040959 (2011).

34 Webb, J. R., Milne, K., Watson, P., Deleeuw, R. J. & Nelson, B. H. Tumor-infiltrating lymphocytes expressing the tissue resident memory marker CD103 are associated with increased survival in high-grade serous ovarian cancer. *Clin Cancer Res* 20, 434-444, doi:10.1158/1078-0432.CCR-13-1877 (2014).

35 Webb, J. R., Milne, K. & Nelson, B. H. PD-1 and CD103 Are Widely Coexpressed on Prognostically Favorable Intraepithelial CD8 T Cells in Human Ovarian Cancer. *Cancer Immunol Res* 3, 926-935, doi:10.1158/2326-6066.CIR-14-0239 (2015).

36 Djenidi, F. *et al.* CD8+CD103+ tumor-infiltrating lymphocytes are tumor-specific tissue-resident memory T cells and a prognostic factor for survival in lung cancer patients. *J Immunol* 194, 3475-3486, doi:10.4049/jimmunol.1402711 (2015).

37 Edwards, J. *et al.* CD103+ tumor-resident CD8+ T cells are associated with improved survival in immunotherapy naive melanoma patients and expand significantly during anti-PD1 treatment. *Clin Cancer Res*, doi:10.1158/1078-0432.CCR-17-2257 (2018).

38 Santegoets, S. J. *et al.* The Anatomical Location Shapes the Immune Infiltrate in Tumors of Same Etiology and Affects Survival. *Clin Cancer Res* 25, 240-252, doi:10.1158/1078-0432.ccr-18-1749 (2019).

39 Hutloff, A. *et al.* ICOS is an inducible T-cell co-stimulator structurally and functionally related to CD28. *Nature* 397, 263-266, doi:10.1038/16717 (1999).

40 Burris, H. A. *et al.* Phase 1 safety of ICOS agonist antibody JTX-2011 alone and with nivolumab (nivo) in advanced solid tumors; predicted vs observed pharmacokinetics (PK) in ICONIC. *Journal of Clinical Oncology* 35, 3033-3033, doi:10.1200/JCO.2017.35.15_suppl.3033 (2017).

41 Fergusson, J. R. *et al.* CD161 defines a transcriptional and functional phenotype across distinct human T cell lineages. *Cell Rep* 9, 1075-1088, doi:10.1016/j.celrep.2014.09.045 (2014).

42 Fergusson, J. R. *et al.* CD161(int)CD8+ T cells: a novel population of highly functional, memory CD8+ T cells enriched within the gut. *Mucosal Immunol* 9, 401-413, doi:10.1038/mi.2015.69 (2016).

43 Thommen, D. S. *et al.* A transcriptionally and functionally distinct PD-1(+) CD8(+) T cell pool with predictive potential in non-small-cell lung cancer treated with PD-1 blockade. *Nat Med*, doi:10.1038/s41591-018-0057-z (2018).

44 Kansy, B. A. *et al.* PD-1 Status in CD8(+) T Cells Associates with Survival and Anti-PD-1 Therapeutic Outcomes in Head and Neck Cancer. *Cancer Res* 77, 6353-6364, doi:10.1158/0008-5472.can-16-3167 (2017).

45 Kim, H. D. *et al.* Association Between Expression Level of PD1 by Tumor-Infiltrating CD8(+) T Cells and Features of Hepatocellular Carcinoma. *Gastroenterology* 155, 1936-1950.e1917, doi:10.1053/j.gastro.2018.08.030 (2018).

46 Middha, S. *et al.* Majority of B2M-Mutant and -Deficient Colorectal Carcinomas Achieve Clinical Benefit From Immune Checkpoint Inhibitor Therapy and Are Microsatellite Instability-High. *JCO precision oncology* 3, doi:10.1200/po.18.00321 (2019).

47 Kotecha, N., Krutzik, P. O. & Irish, J. M. Web-based analysis and publication of flow cytometry experiments. *Curr Protoc Cytom* Chapter 10, Unit10 17, doi:10.1002/0471142956.cy1017s53 (2010).

48 Hollt, T. *et al.* Cytosplore: Interactive Immune Cell Phenotyping for Large Single-Cell Datasets. *EuroVis* 35 (2016).

49 Pezzotti, N., Höllt, T., Lelieveldt, B., Eisemann, E. & Vilanova, A. Hierarchical Stochastic Neighbor Embedding. *Computer Graphics Forum* 35, 21-30, doi:10.1111/cgf.12878 (2016).

50 van Unen, V. *et al.* Visual analysis of mass cytometry data by hierarchical stochastic neighbour embedding reveals rare cell types. *Nat Commun* 8,

1740, doi:10.1038/s41467-017-01689-9 (2017).

51 Abdelaal, T. *et al.* Predicting cell populations in single cell mass cytometry data. *Cytometry A*, doi:10.1002/cyto.a.23738 (2019).

52 Johnson, W. E., Li, C. & Rabinovic, A. Adjusting batch effects in microarray expression data using empirical Bayes methods. *Biostatistics* 8, 118-127, doi:10.1093/biostatistics/kxj037 (2006).

53 Butler, A., Hoffman, P., Smibert, P., Papalexi, E. & Satija, R. Integrating single-cell transcriptomic data across different conditions, technologies, and species. *Nat Biotechnol*, doi:10.1038/nbt.4096 (2018).

54 Waltman, L. & van Eck, N. J. A smart local moving algorithm for large-scale modularity-based community detection. *The European Physical Journal B* 86, 471, doi:10.1140/epjb/e2013-40829-0 (2013).

55 van der Maaten, L. J. P. & Hinton, G. E. Visualizing high-dimensional data using t-SNE. *J. Mach. Learn. Res.* 9, 2579-2605 (2008).

56 Ijsselsteijn, M. E. *et al.* Cancer immunophenotyping by seven-color multispectral imaging without tyramide signal amplification. *The journal of pathology. Clinical research* 5, 3-11, doi:10.1002/cjp2.113 (2019).

SUPPLEMENTAL METHODS

Tissue digestion and cell isolation

Tumor tissues, tumor-associated lymph nodes, and colorectal healthy mucosa were collected in IMDM+Glutamax medium (Gibco) complemented with 20% fetal calf serum (FCS) (Greiner Bio-One) after surgical resection. Samples were cut into small fragments in a petri dish, and enzymatically digested with 1 mg/mL collagenase D (Roche Diagnostics) and 50 µg/mL DNase I (Roche Diagnostics) in 5 mL of IMDM+Glutamax medium for 30 min at 37°C in gentleMACS C tubes (Miltenyi Biotec). During and after incubation, cell suspensions were mechanically dissociated on the gentleMACS Dissociator (Miltenyi Biotec). Cell suspensions were filtered through a 70-µm cell strainer (Corning) and washed in IMDM+Glutamax medium. Cell number and viability was determined with the Muse Count & Viability Kit (Merck) on the Muse Cell Analyzer (Merck). Cells were cryopreserved based on the number of viable cells in liquid nitrogen until time of analysis in 50% FCS and 10% dimethyl sulfoxide (DMSO) (Merck). Peripheral blood mononuclear cells (PBMCs) were isolated by Ficoll-Paque (provided by apothecary LUMC) density-gradient centrifugation and cryopreserved in liquid nitrogen until time of analysis in 20% FCS and 10% DMSO.

Mass cytometry antibodies

Heavy metal isotope-tagged monoclonal antibodies are listed in **Table S2**. Purified antibodies were conjugated with heavy metal reporters in-house using the MaxPar X8 Antibody Labeling Kit (Fluidigm) according to the manufacturer's instructions. All antibodies were titrated to determine the optimal labelling concentration.

Mass cytometry antibody staining and data acquisition

Percoll (GE Healthcare) density-gradient centrifugation was performed to isolate immune cells from tumor tissues and colorectal healthy mucosa. Cells were washed in Maxpar Cell Staining Buffer (CSB, Fluidigm), and incubated with 1 mL CSB containing 1 µM Cell-ID intercalator-^{103}Rh (Fluidigm) for 15 min at room temperature (rT). Cells were washed, incubated with human Fc receptor block (BioLegend) for 10 min at rT, and stained with cell surface antibodies for 45 min at rT in a final volume of 100 uL. After washing, cells were incubated with 1 mL Maxpar Fix and Perm buffer (Fluidigm Sciences) containing 0.125 µM Cell-ID intercalator-Ir (Fluidigm) overnight at 4°C. Cells were acquired on a Helios-upgraded CyTOF2 and Helios mass cytometer (Fluidigm) at an event rate of <500 events/sec in de-ionized water containing 10x diluted EQ Four Element Calibration Beads (Fluidigm). Data were normalized with the normalization passport EQ-P13H2302_ver2 for each experiment.

Mass cytometry data analysis

Correlation analysis of the presence of immune cell clusters across samples (**Figure 7**) was performed using Spearman's rank correlation in the Corrplot R package. PD-1 subsets in CRCs (**Figure S9**) were gated based on a healthy control PBMC sample into PD-1 negative cells (no PD-1 expression), PD-1 intermediate cells (PD-1 expression levels to a similar extent as healthy control PBMCs), and PD-1 high cells (PD-1 expression levels surpassing that of healthy control PBMCs) as described in a previous study on functional diversity between PD-1 subsets.[43] Tumors with less than 100 cells in one of the PD-1 subsets were excluded from this analysis. Sample and immune cell cluster t-distributed Stochastic Neighbor Embedding (t-SNE) maps (**Figure S8**) were computed as described previously.[57]

Flow cytometry antibody staining

Cells were first incubated with human Fc receptor block and cell surface antibodies for 45 min at 4°C. After washing, cells were stained for intracellular proteases and cytokines using Fixation Buffer and Intracellular Staining Perm Wash Buffer (BioLegend) or for FOXP3 expression using FOXP3 Transcription Factor Staining Buffer Set (eBioscience). Compensation was carried out with CompBeads

(BD Biosciences) and ArC reactive beads (Life Technologies). Cells were acquired on a LSR II and LSR Fortessa flow cytometer (BD Biosciences) running FACSDiva software version 8.0 (BD Biosciences). Data were analyzed with FlowJo software version 10.2 (Tree Star Inc). Antibody details are listed in **Table S3**.

Immunohistochemical staining

FFPE blocks from colorectal cancers (CRCs) were obtained from the department of Pathology at the Leiden University Medical Center (Leiden, The Netherlands). Tumor mismatch repair (MMR) status (MMR-proficient or MMR-deficient) was determined by immunohistochemical detection of PMS2 (anti-PMS2 antibodies; clone EP51, DAKO) and MSH6 (anti-MSH6 antibodies; clone EPR3945, Abcam) proteins.[58] MMR-deficiency was determined by lack of expression of at least one of the MMR-proteins in the presence of an internal positive control. Immunohistochemical detection of human leukocyte antigen (HLA) class I expression was performed with HCA2 and HC10 monoclonal antibodies (Nordic-MUbio), and classified as HLA class I positive, weak, or loss as described previously[32].

Multispectral immunofluorescence detection

Five-µm frozen tissue sections were cut on adhesive immunohistochemistry slides. Following fixation in ice-cold 100% methanol for 5 min and wash in PBS, the tissues were incubated with Superblock buffer (Thermo Fisher Scientific) for 30 min at rT. For the detection of CD127, TSA signal amplification was performed with Opal520 from the Opal 7-color manual IHC kit (Perkin Elmer), according to manufacturer's instructions. Thereafter, the tissues were incubated with primary TCR V beta F1 and CD45RO antibodies to be detected indirectly overnight at rT, followed by incubation with corresponding fluorescent secondary antibodies CF680 and CF633, respectively, for 1h at rT. The tissues were then incubated with directly conjugated primary CD3-AF594 and CD7-AF647 antibodies for 5h at rT. CD3 was conjugated to AF594 using the Alexa Fluor 594 antibody labelling kit (Thermo Fisher Scientific). Lastly, the tissues were incubated with 1 µM DAPI for nuclear counterstaining, and mounted with Prolong® Gold Antifade Reagent (Cell Signaling Technology). Antibody details are listed in **Table S4**.

REFERENCES

57 van Unen, V. *et al.* Mass Cytometry of the Human Mucosal Immune System Identifies Tissue- and Disease-Associated Immune Subsets. *Immunity* 44, 1227-1239, doi:10.1016/j.immuni.2016.04.014 (2016).

58 Hall, G. *et al.* Immunohistochemistry for PMS2 and MSH6 alone can replace a four antibody panel for mismatch repair deficiency screening in colorectal adenocarcinoma. *Pathology* 42, 409-413, doi:10.3109/00313025.2010.493871 (2010).

SUPPLEMENTAL FIGURES

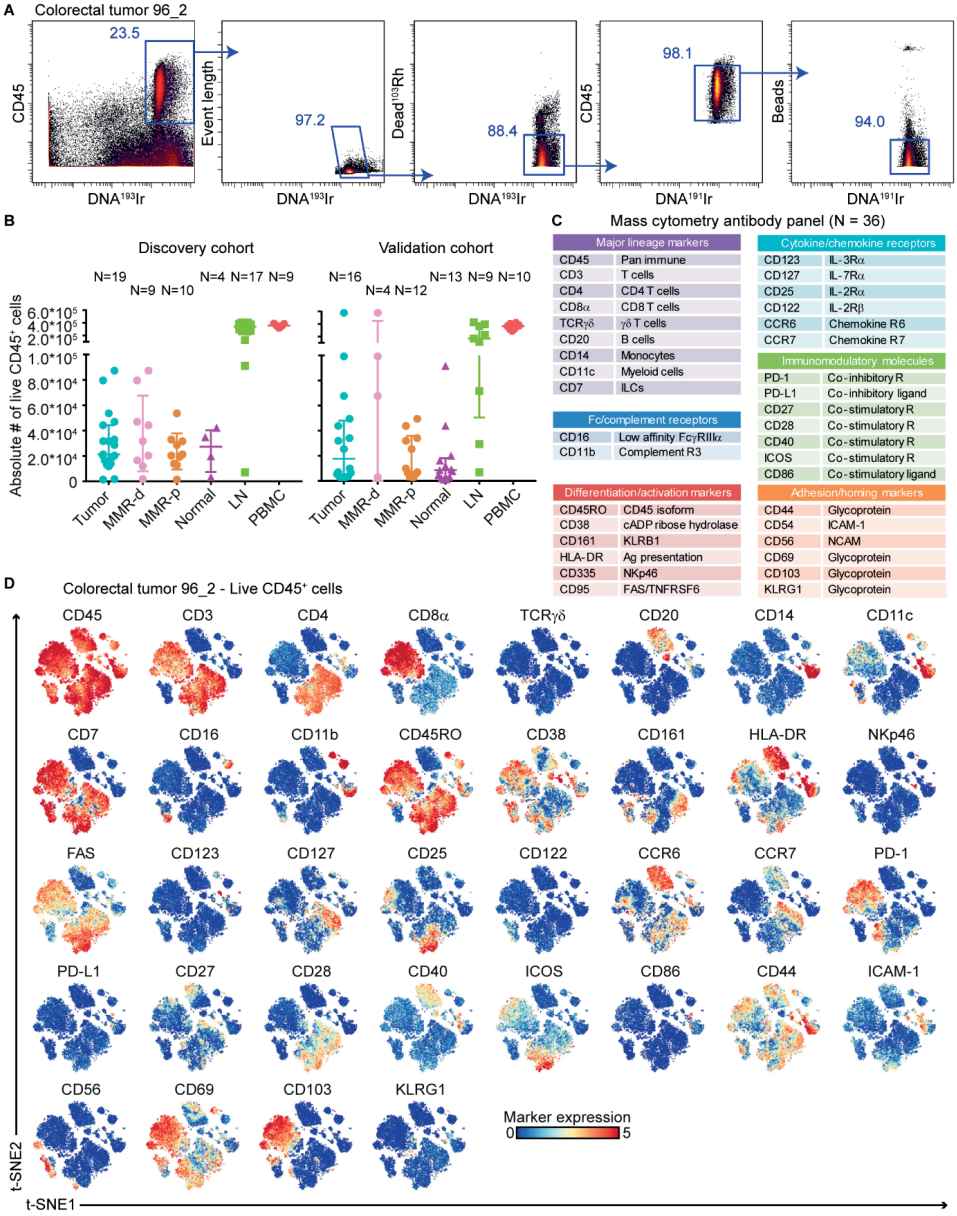

Figure S1. Mass cytometry gating strategy and antibody expression patterns.
A. Mass cytometry gating strategy for single, live CD45⁺ cells of a representative colorectal tumor sample showing sequential gates with percentages. **B.** Absolute number of live CD45⁺ cells of CRC tissues, colorectal healthy mucosa, tumor-associated lymph nodes, and peripheral blood samples of the discovery and validation cohort of CRC patients. Bars indicate median ± IQR. Each dot represents an individual sample. Data from 22 independent experiments with mass cytometry. **C.** Markers used to characterize immune cell phenotypes by mass cytometry. **D.** t-SNE embedding showing marker expression patterns of each antibody on single, live CD45⁺ cells ($2.0*10^4$) from the same tumor sample as shown in (**A**). Each dot represents a single cell. All markers are shown with an expression range of 0-5, with the exception of CD86 (0-3) due to lower sensitivity of the metal (^{115}In).

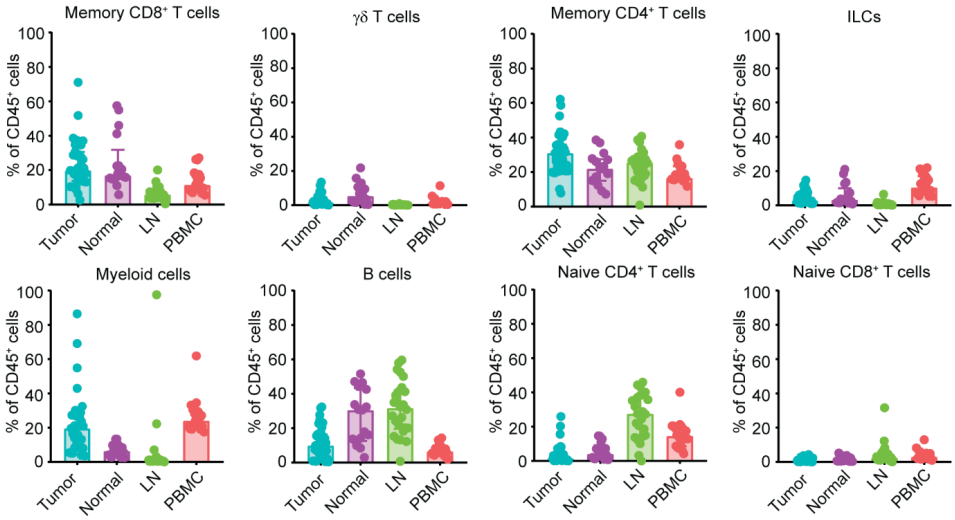

Figure S2. Major immune lineage frequencies in different tissue types of colorectal cancer patients.
Frequencies of major immune lineages across CRC tissues (N=35), colorectal healthy mucosa (N=17), tumor-associated lymph nodes (N=26), and peripheral blood (N=19) as percentage of total CD45⁺ cells. Bars indicate median ± IQR. Each dot represents an individual sample. Data from 22 independent experiments with mass cytometry.

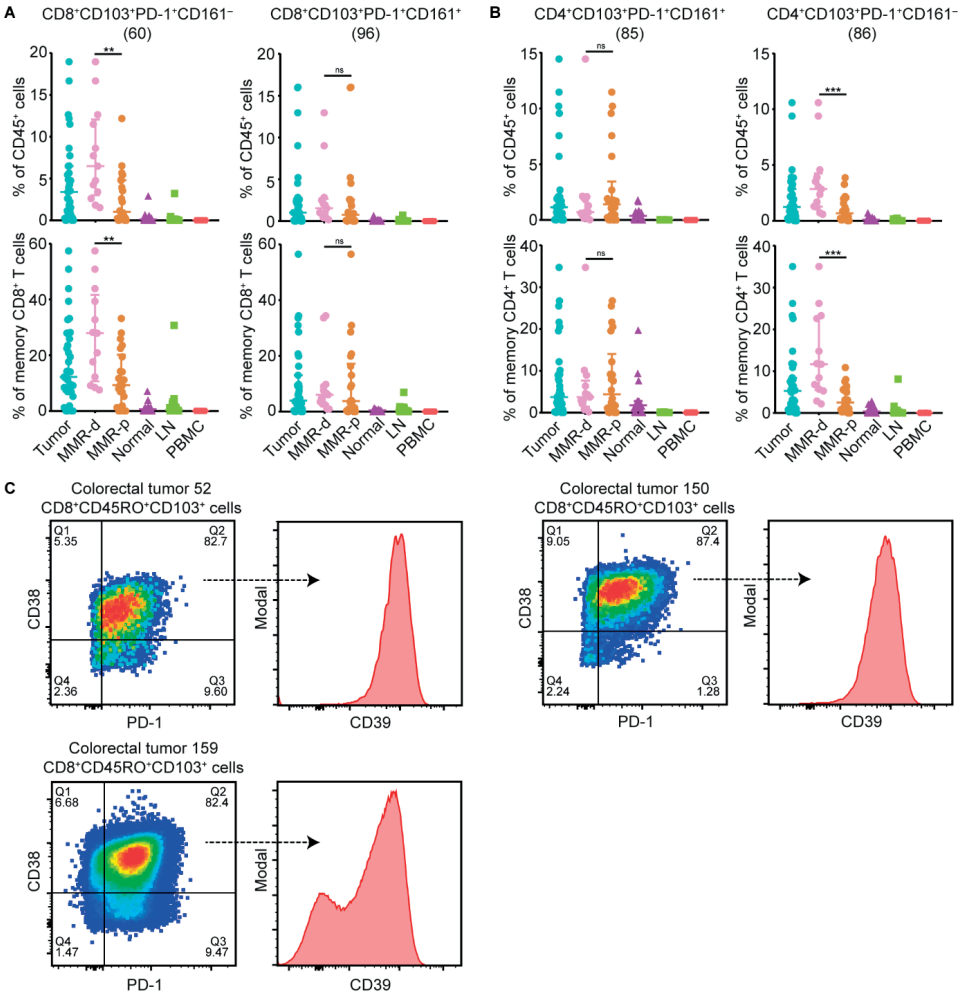

Figure S3. Characterization of tumor tissue-specific immune cell clusters corresponding to Figure 2 and 3.
A and B. Frequencies of CD103+PD-1+CD161− and CD103+PD-1+CD161+ memory CD8+ T cells (**A**) and CD4+ T cells (**B**) among CRC tissues (N=35, further subdivided into MMR-deficient (N=13) and MMR-proficient (N=22)), colorectal healthy mucosa (N=17), tumor-associated lymph nodes (N=26), and peripheral blood (N=19) as percentage of total CD45+ cells (upper panel) and memory CD8+ or CD4+ T cells (lower panel). Cluster IDs correspond to the ones in **Figure 2B** and **Figure 3B**. Bars indicate median ± IQR. Each dot represents an individual sample. Data from 22 independent experiments with mass cytometry. NS, not significant, ***P*<0.01, ****P*<0.001 by Mann-Whitney U test. **C.** Flow cytometry plots of colorectal tumors (N=3) showing the expression of CD39 within CD8+CD45RO+CD103+PD-1+CD38+ cells.

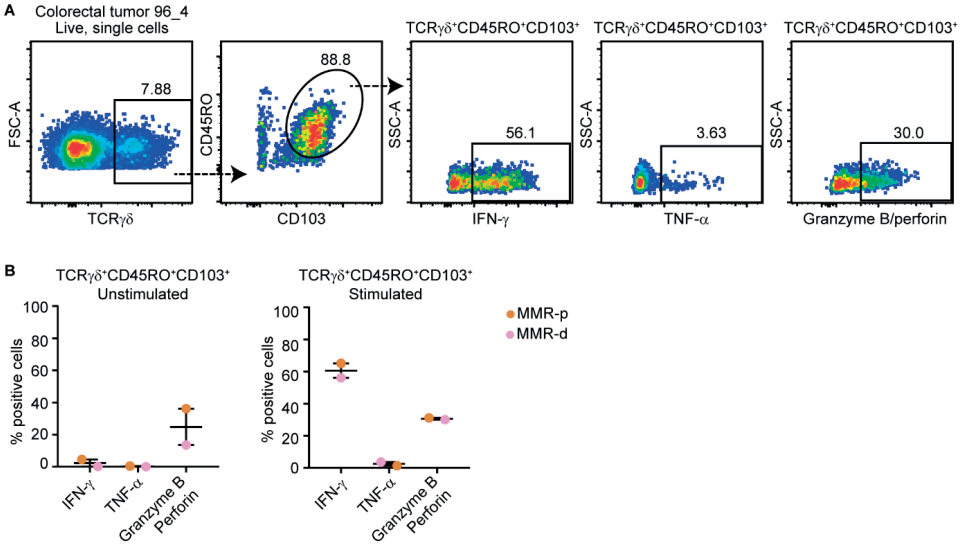

Figure S4. Tumor-resident γδ T cells are capable of producing cytokines and cytotoxic molecules upon stimulation.

A. Flow cytometry plots of a MMR-deficient tumor sample showing the expression of cytokines and cytotoxic molecules by TCRγδ+CD45RO+CD103+ cells upon stimulation with PMA/ionomycin. **B.** IFN-γ, TNF-α, and granzyme B/perforin expression by TCRγδ+CD45RO+CD103+ cells from a MMR-deficient and MMR-proficient CRC with and without stimulation with PMA/ionomycin. Bars indicate median ± IQR. Each dot represents an individual sample.

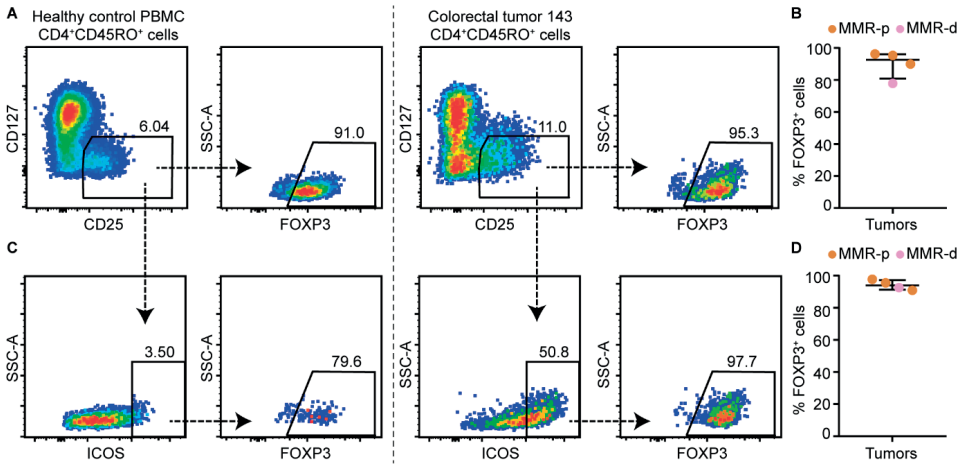

Figure S5. Expression of FOXP3 by ICOS+ regulatory T cells in colorectal tumors.

A. Representative plots of a healthy control PBMC sample and a MMR-proficient tumor sample analyzed by flow cytometry showing the expression of FOXP3 by regulatory T cells ($CD25^+CD127^{low}$). **B.** FOXP3 expression in regulatory T cells ($CD25^+CD127^{low}$) from CRC tissues (N=4, of which 1 MMR-deficient and 3 MMR-proficient). Bars indicate median ± IQR. Each dot represents an individual sample. Data from two independent experiments with flow cytometry. **C.** Representative plots of a healthy control PBMC sample and a MMR-proficient tumor sample analyzed by flow cytometry showing the expression of FOXP3 by $ICOS^+$ regulatory T cells ($CD25^+CD127^{low}$). **D.** FOXP3 expression in $ICOS^+$ regulatory T cells ($CD25^+CD127^{low}$) from CRC tissues (N=4, of which 1 MMR-deficient and 3 MMR-proficient). Bars indicate median ± IQR. Each dot represents an individual sample. Data from two independent experiments with flow cytometry.

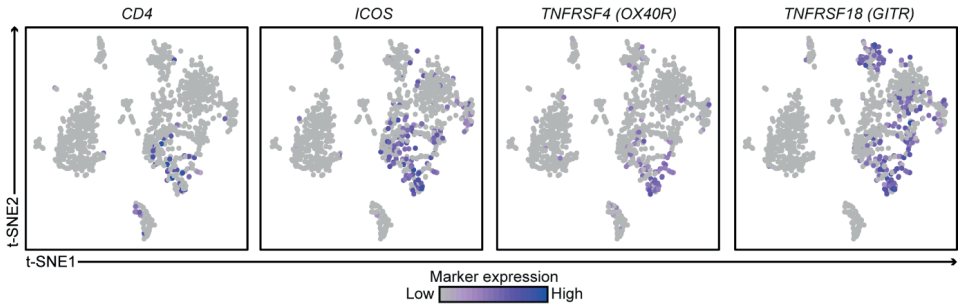

Figure S6. Co-expression of *ICOS*, *TNFRSF4 (OX40R)*, and *TNFRSF18 (GITR)* on CD4⁺ T cells in colorectal cancers.
t-SNE embedding showing 1,079 cells from CRC tissues (N=7) analyzed by single-cell RNA-sequencing. Colors represent the log-transformed expression levels of indicated markers. Each dot represents a single cell.

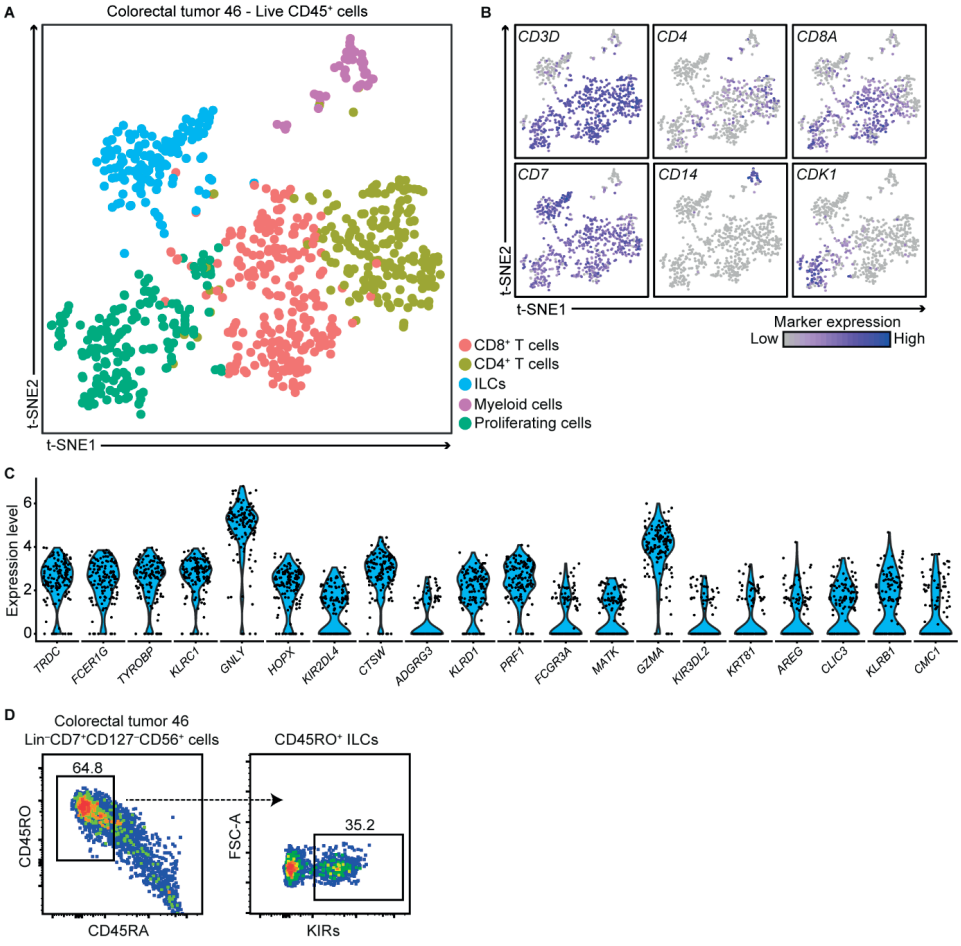

Figure S7. Expression of cytotoxic molecules and KIRs by tumor-resident ILCs.
A and B. t-SNE embedding of single-cell RNA-sequencing data showing 795 cells from one MMR-deficient tumor that was selected for its high numbers of Lin⁻CD7⁺CD127⁻CD56⁺CD45RO⁺ ILCs (70% of the ILC cluster) based on mass cytometry data. Colors represent the different clusters (**A**) and the log-transformed expression levels of indicated

markers (**B**). Each dot represents a single cell. **C.** Violin plot showing log-transformed expression levels of the top 20 differentially expressed genes within ILCs (N=137) as identified in (**A**). Each dot represents a single cell. **D.** Flow cytometry plots showing the cell surface expression of KIRs in Lin$^-$CD7$^+$CD127$^-$CD56$^+$CD45RO$^+$ ILCs from the same tumor as in (**A-C**).

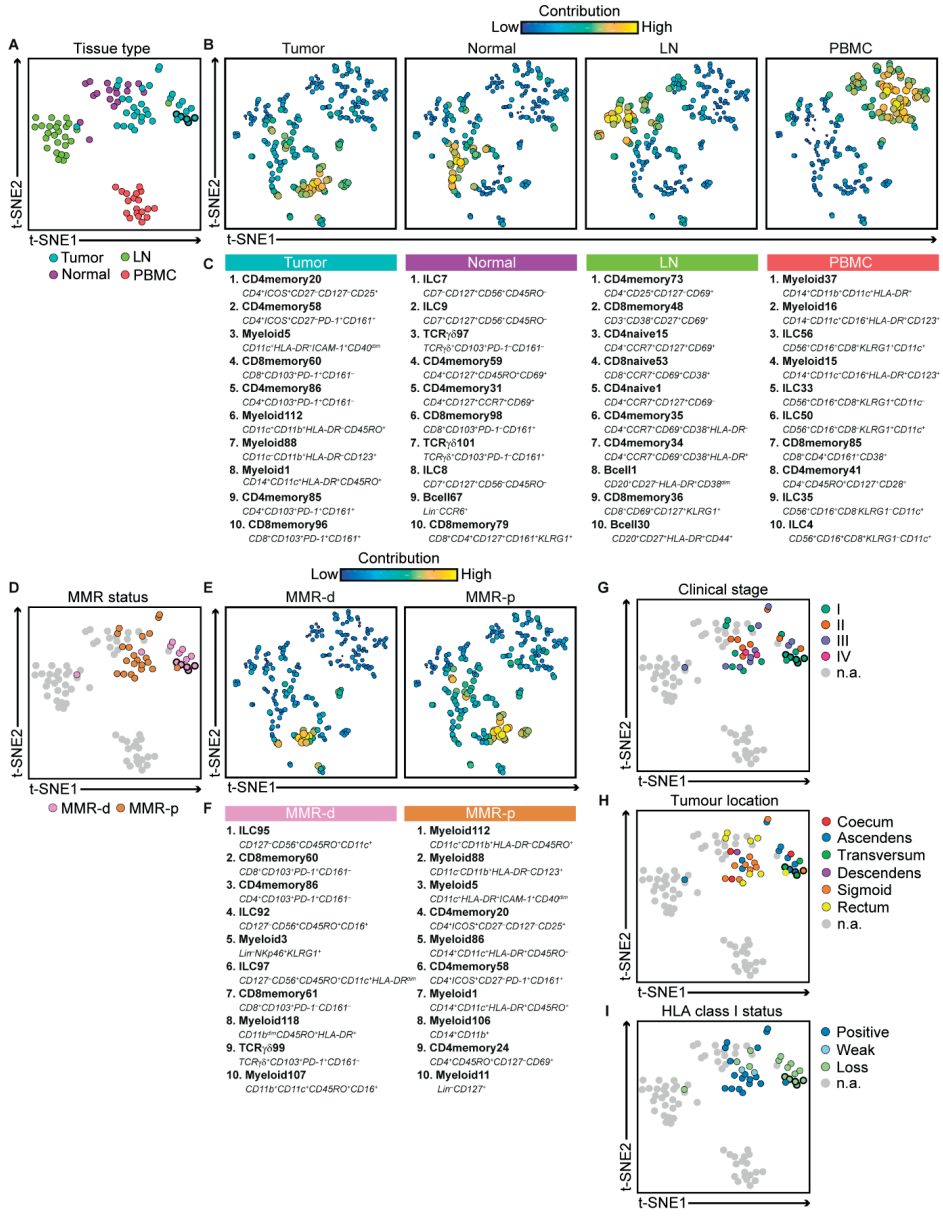

Figure S8. Integrated analysis of the immune composition in different tissue types of colorectal cancer patients.

A. Collective t-SNE analysis showing the clustering of 97 samples based on cell percentage data (of CD45$^+$ cells) of 218 immune cell clusters. Every dot represents a sample colored by tissue type. Five primary tumors at different locations from the same patient are highlighted. One lymph node sample clustered within the tumor samples, and was found to be infiltrated by tumor cells upon histological examination. One tumor sample clustered within the lymph

node samples, and was found to contain large populations of naive CD4+ T cells and B cells, which are enriched in lymph nodes. Histological examination of the tumor confirmed the presence of lymphoid aggregates with germinal centers, a Crohn-like lymphoid reaction that can be a feature of MMR-deficient tumors.[59] **B.** Collective t-SNE analysis showing the clustering of 218 immune cell clusters based on cell percentage data (of CD45+ cells) of 97 samples. Every dot represents an immune cell cluster. Dot color and size indicate the contribution of the immune cell cluster to the respective t-SNE sample signatures as shown in (**A**). **C.** Top ten ranked immune cell clusters contributing to the t-SNE sample signatures as shown in (**A**). Unique cluster IDs and a short description of their phenotype are displayed. **D.** Collective t-SNE analysis of (**A**) colored by MMR status of the tumor samples. **E.** Collective t-SNE analysis of (**B**) showing the contribution of the immune cell clusters to the respective t-SNE sample signatures as shown in (**D**). **F.** Top ten ranked immune cell clusters contributing to the t-SNE sample signatures as shown in (**D**). Unique cluster IDs and a short description of their phenotype are displayed. **G-I.** Collective t-SNE analysis of (**A**) colored by clinical stage (**G**), tumor location (**H**), and HLA class I status (**I**).

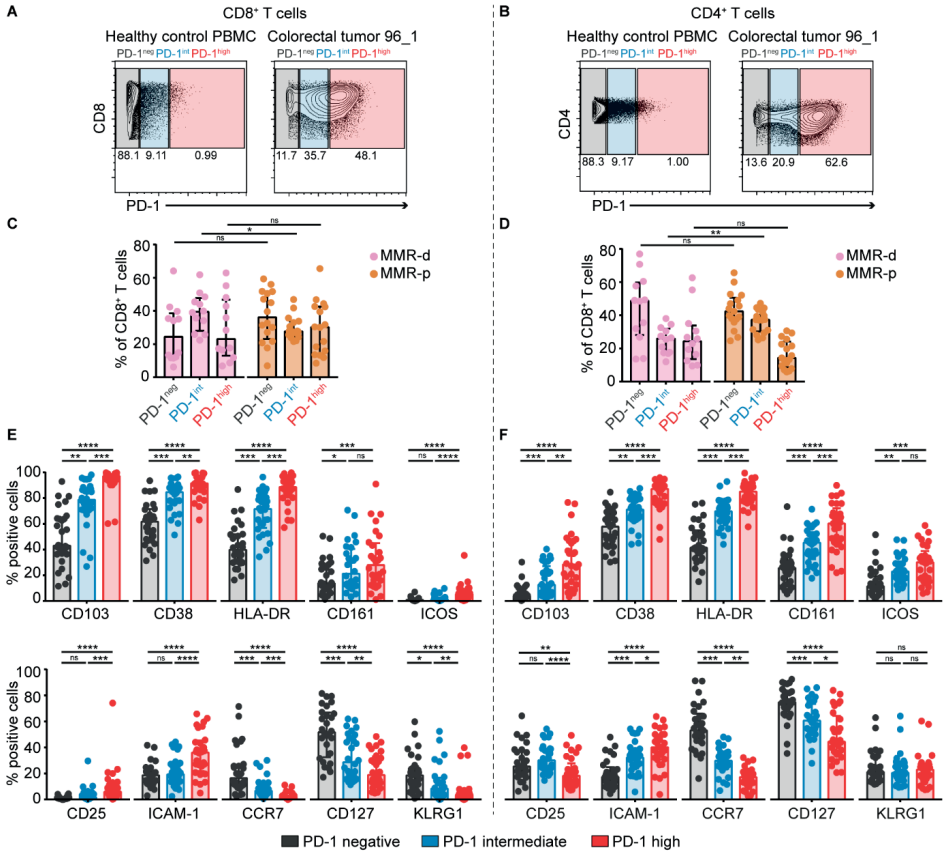

Figure S9. PD-1 expression level of CD8+ and CD4+ T cells correlates with distinct states of activation and differentiation in colorectal tumors.

A and B. Representative plots showing the gating strategy for PD-1 negative, intermediate and high CD8+ T cells (**A**) and CD4+ T cells (**B**) in healthy control PBMC and colorectal tumor tissues (see **Supplemental methods**). **C**. Frequencies of PD-1 negative, intermediate and high CD8+ T cells in MMR-deficient (N=12) and MMR-proficient (N=16) tumors. **D**. Frequencies of PD-1 negative, intermediate and high CD4+ T cells in MMR-deficient (N=12) and MMR-proficient (N=17) tumors. **C**,**D**. Bars indicate median ± IQR. Data from 22 independent experiments with mass cytometry. NS, not significant, **P*<0.05, ***P*<0.01 by Mann-Whitney U-test. **E**. Frequencies of selected immune cell markers expressed by PD-1 negative, intermediate and high CD8+ T cells in CRCs (N=28). **F**. Frequencies of selected immune cell markers expressed by PD-1 negative, intermediate and high CD4+ T cells in CRCs (N=29).

E,**F**. Bars indicate median ± IQR. Each dot represents an individual sample. Data from 22 independent experiments with mass cytometry. NS, not significant, **P*<0.05, ***P*<0.01, ****P*<0.001, *****P*<0.0001 by Friedman test with Dunn's test for multiple comparisons.

REFERENCES

59 Graham, D. M. & Appelman, H. D. Crohn's-like lymphoid reaction and colorectal carcinoma: a potential histologic prognosticator. *Mod Pathol* 3, 332-335 (1990).

SUPPLEMENTAL TABLES

The supplementary tables are available in the online version of this manuscript at http://dx.doi.org/10.1136/gutjnl-2019-318672 and in the appendix to this thesis at the repository of Leiden University (https://hdl.handle.net/1887/3439882).

Table S1: Overview of clinical samples and patient characteristics.
Table S2: Antibodies used for mass cytometry experiments.
Table S3: Antibodies used for flow cytometry and cell sorting experiments.
Table S4: Antibodies used for multispectral immunofluorescence detection.
Table S5: Coefficient and *P*-values of immune cell correlations observed in colorectal cancer tissues (corresponding to Figure 7).